

# RECENT DEVELOPMENT OF DUPLEX STAINLESS STEELS

*J.-O. Nilsson, G. Chai, U. Kivisäkk*

*R&D Centre, Sandvik Materials Technology, Sweden*

## **Abstract**

Recent development of duplex stainless steels is described. The advent of SAF 2707 HD, a 27Cr-7Ni-5Mo-0.4N duplex steel, shows that it is possible to reach a PRE-value close to 50 without sacrificing the fabricability. Modern methods for simulating the interaction between ferrite and austenite intimates that the steels of tomorrow may be optimized with respect to mechanical as well as corrosion properties. Methods under development presented here are multi-scale modelling of plastic deformation and high resolution electrochemical techniques.

## **Introduction**

Duplex stainless steels (DSS) were first described by Bain and Griffiths in 1927 but it was not until the 1930's that duplex stainless steels (DSS) became commercially available. About 80 years have passed since the first discovery but DSS are still under development. The interest in DSS in recent years derives from the high resistance of newly developed high alloy DSS to chloride induced corrosion. As a matter of fact it is the combination of several properties such as corrosion resistance, mechanical properties, weldability and price that makes the DSS unrivalled in many applications [1, 2].

Despite the attractiveness of DSS they have limitations. 475°C-embrittlement sets an upper limit to the temperature range recommended during service. Improper welding or production may cause precipitation of  $\sigma$ -phase or chromium nitrides resulting in deteriorated mechanical properties and/or corrosion properties. The endeavour to design gradually more corrosion resistant DSS provides a driving force to add more chromium, molybdenum and nitrogen, all of which destabilize the microstructure and promote formation of precipitates. The conflict between microstructural stability on one hand and the incentive to add more alloying elements on the other is a challenge to the designer of the alloys of tomorrow.

The characteristic features of DSS, whether it is plastic deformation or corrosion, derive from the interplay between the two constituents ferrite and austenite. With the aid of modern computational tools it has become possible to predict microstructures with great precision and also simulate plastic deformation in a two-phase material such as a DSS. We therefore have powerful tools for simulating this interaction as a means of optimising corrosion and mechanical properties.

## **Trends in the development of DSS**

Two trends in the development of DSS may be identified; one towards lean nickel-poor DSS and one towards highly alloyed so called super duplex stainless steels (SDSS). One advantage of lean DSS is the paucity of nickel, the price of which is high and also shows enormous fluctuations.

However, if a high resistance to pitting corrosion is required significant amounts of the ferrite stabilizers chromium and molybdenum have to be used which sets a lower limit as regards the nickel concentration.

The SDSS UNS S32750, S32760 and S32520 with a PRE-value of about 42 were introduced more than 15 years ago. It was thought that SDSS with a PRE-value well above 42 were remote but very recently a SDSS having a PRE-umber close to 50 has been launched. Existing SDSS have shown some limitations in high temperature sea water. Therefore, there has been a need on the market of a DSS with improved resistance to pitting corrosion. SAF 2707 was developed to meet this need and provided a leap in performance. The nominal composition of this alloy together with SAF 2507 is shown in Table 1 below.

Table 1. Nominal chemical composition of two super duplex stainless steels

Grade	UNS	Cmax	Cr	Ni	Mo	N	PRE
SAF 2507	S32750	0.03	25	7	4	0.3	42
SAF 2707HD	S32707	0.03	27	7	5	0.4	49

The comparison in Figure 1 shows that the pitting resistance is significantly improved in SAF 2707 compared to SAF 2507. The tests used in this comparative study was a modified version of the ASTM G48 test and a crevice corrosion test in 6% FeCl<sub>3</sub> according to the MTI-2 procedure [3]. Critical pitting temperatures (CPT) can also be measured using potentiostatic tests at +600mV. The CPT as a function of the concentration of sodium chloride in the range 3-25% is shown in Figure 2. It is quite apparent that SAF 2707 HD is superior to SAF 2507 in the entire concentration range.

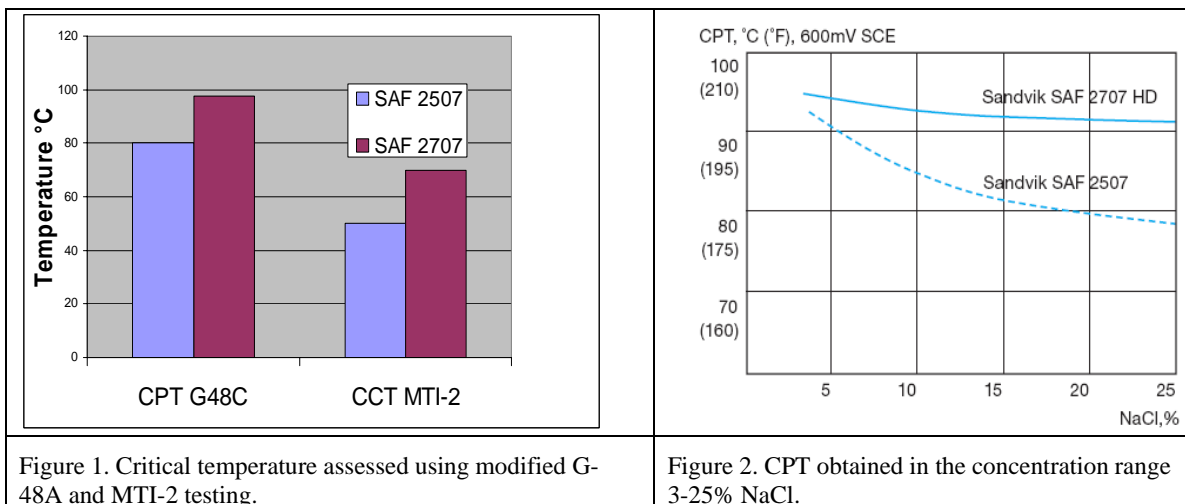


Figure 1. Critical temperature assessed using modified G-48A and MTI-2 testing.

Figure 2. CPT obtained in the concentration range 3-25% NaCl.

## Material modelling of micro mechanical behaviour in DSS

Since the austenitic phase and the ferritic phase have different chemical, physical and mechanical properties, these phases behave differently at the microstructural level. Each phase respond differently to the environments such as corrosion, thermal cycle and loading. For example, the load sharing between the individual phases during loading is different due to the differences in the modulus of elasticity and deformation hardening rate of the individual phases. Strong inter-phase reactions will also result in the formation of micro stresses that maintain their equilibrium among subsets of grains of different orientations [4]. These residual micro stresses can have great effects on SCC, yielding and damage of the material, and consequently affect their strength, deformation and fracture behaviour [5, 6]. Understanding the micromechanical

reactions is therefore important for the application of the duplex stainless steels and for alloy design and material development.

It is difficult to measure the stress-strain behaviour of the individual phases in DSS by the conventional mechanical testing methods due to its fine and heterogeneous microstructure. In-situ diffraction methods using X-ray, synchrotron and neutron are now used to analyze the load sharing, stress interaction between phases and grains and consequently the micro stress-strain behaviour of DSS [4, 7]. Hardness is a measure of the material resistance to plastic deformation. This indicates that the hardness (micro or nano) method can also be used to estimate plastic deformation hardening rate if the size of the austenitic and ferritic phase is sufficient [6].

In recent years, multi-scale material modelling has gained much interest from the researchers in the field of material mechanics. This type of modelling offers the possibility to study the behaviour of single phases, single grains and load sharing between the phases in a multi-phase material. The basic idea in multi-scale material modelling is that the a priori homogenized macro-scale material model is replaced by the homogenized response of a representative volume element (RVE) as shown in Figure 3. Multi-scale material modelling uses micro-scale crystal plasticity and continuum models [6]. Figure 4 shows the results of the multi-scale material modelling for SAF 2507 bar material in as delivered condition; 2507AD during static tensile testing. The ferritic phase is a stronger phase at a total strain less than about 3% and then becomes a softer phase with increasing strain. These observations are similar to the results from the experimental observations as shown in [6].

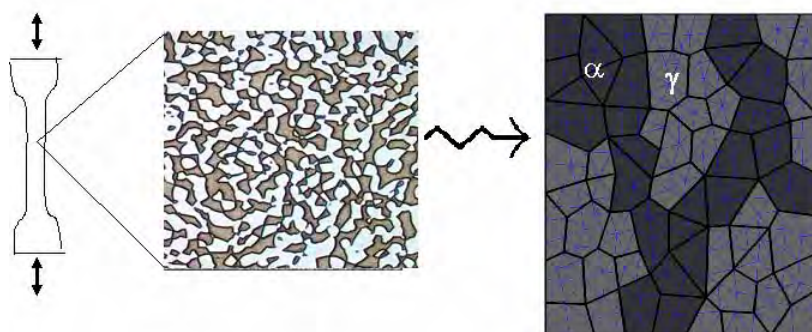
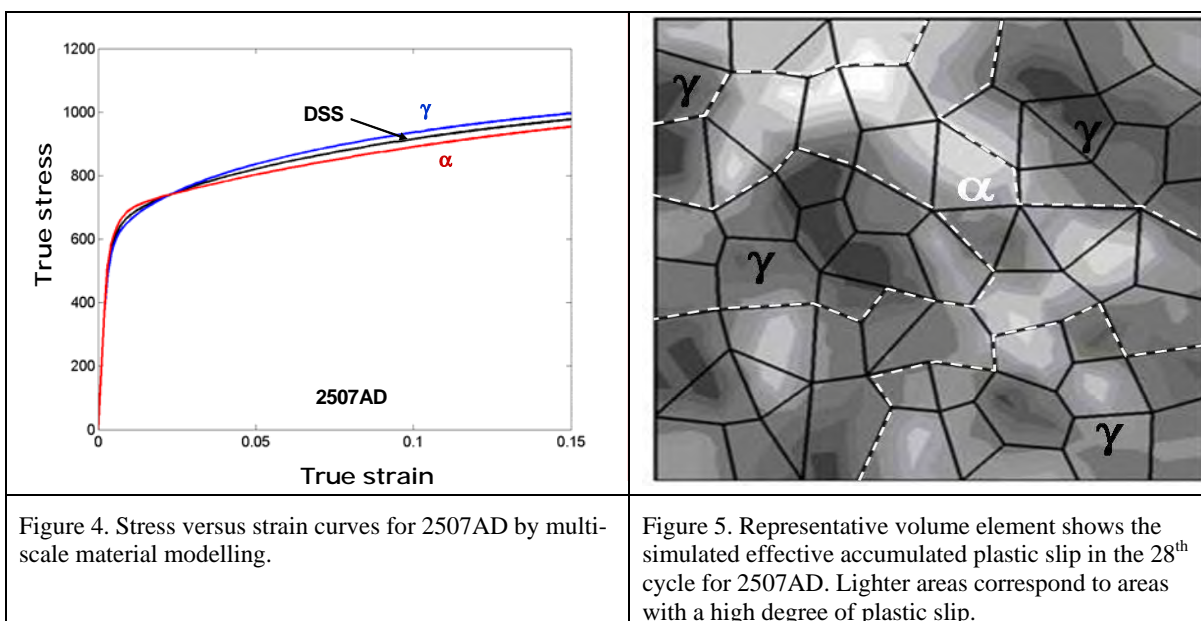


Figure 3. Multi-scale material modelling of duplex stainless steels

Fatigue is a progressive process. The early stage of fatigue damage is the permanent substructural and microstructural changes (strain localization) and creation of microscopic cracks. Fatigue damage is indicated by the formation of persistent slip bands (PSB) on the meso-micro scales and the subsequent crack initiation. Although much work has been done concerning two-phase or multi-phase metals, it is not clear in which phase or how fatigue damage occurs in these metals. Multi-scale material modelling provides the possibility to study the behaviour of single phases, single grains and load sharing between the phases in a multi-phase material as shown [6].

During cyclic strain loading, DSS materials usually have hardening and then softening processes. The simulations using the multi-scale material modelling show that hardening and softening processes also occur in the austenitic and ferritic phases [6], but behave differently. The ferritic phase has a shorter cyclic hardening period and lower hardening rate compared with the austenitic phase. In this paper, micro material damage is defined as the formation of slip bands in

the individual phases. Figure 5 shows the micro damage behaviour in 2507AD due to cyclic loading. The accumulated effective plastic slips are mainly in the ferritic phase, but can also be observed in the austenitic phase. This can be explained by the fact that the damage in 2507AD may start in the austenitic phase but finally dominates in the ferritic phase since the weaker phase is the first to become damaged. This indicates that damage and crack initiation in a two-phase alloy depend not only on the initial strength of the individual phases, but also their deformation hardening behaviour. The final damage and crack initiation may occur in the weakest phase.



## Corrosion properties

The corrosion properties of duplex stainless steel depend upon the chemical composition as well as the degree of homogeneity of alloying elements. In an entirely austenitic stainless steel the distribution of elements is very homogeneous. However, a complication arises in DSS, in which chromium and molybdenum are partitioned to the ferrite and nitrogen is partitioned to the austenite. As a consequence, the PREN value [8] and the associated resistance to pitting may become notably different in the two phases. This problem in DSS can be circumvented by choosing an annealing temperature at which PREN are equal in austenite and ferrite, whereby equal pitting resistance in ferrite and austenite ensues [9].

As mentioned before  $\sigma$ -phase can be formed in DSS leading to a decrease in corrosion resistance. However, a finite amount of  $\sigma$ -phase is required to reduce the pitting corrosion significantly. In a previous investigation [10] the influence of various amounts of  $\sigma$ -phase on the pitting corrosion behaviour of Sandvik SAF 2507 and Sandvik SAF 2906 was made. It is shown that about 1% of  $\sigma$ -phase is necessary to significantly deteriorate the pitting corrosion resistance of Sandvik SAF 2507 and Sandvik SAF 2906. Qualitatively similar results have been reported by others for super duplex stainless steels [11]. In seawater Sandvik SAF 2507 with 6%  $\sigma$ -phase has passed a test at 35°C [12]. Similar results have been found for UNS S32760 for which pitting was observed in chlorinated seawater at 35°C with 6%  $\sigma$ -phase while no pitting was observed at 1.5% [13].

Modern electrochemical techniques offer a means of investigating the corrosion properties of DSS. The advantage of these techniques is that the potential (Scanning probe force microscopy

(SKPFM)), or current distribution (electrochemical scanning tunnelling microscopy technique (EC-STM)), can be mapped with  $\mu\text{m}$  resolution. Since an AFM is used for the SKPFM this enables magnetic force microscopy (MFM) to be used to identify in which phase the measurements are performed. Hence, the corrosion properties of each phase in the DSS as well as galvanic interactions can be studied. The general corrosion properties of DSS have been studied in 1 M and 4 M  $\text{H}_2\text{SO}_4$  with 1 M NaCl with both EC-STM and SKPFM. The austenite was found to be more noble than the ferrite and consequently more pronounced dissolution of ferrite was observed [14, 15].

## Modelling of microstructures

The advent of thermodynamically based computer programs such as Thermo-Calc provided powerful tools for developing new alloys during the 1980's. In fact, SAF 2507 was the first alloy ever to be developed and optimised using computerized techniques that later became known as Thermo-Calc [16]. The main achievement was to define a combination of temperature and composition that led to equal PRE and consequently equal pitting resistance in both phases. The development of SAF 2507 therefore provides a milestone in alloy development, not only within Sandvik but in the steel industry in general.

The techniques have since been refined and developed further to include also DICTRA [17], a computer based tool by which diffusion controlled phase transformations can be modelled. Both programs are dependent upon experimental data such as activities, equilibrium tie lines, solubilities, diffusivities and surface energies. It is very often the case that the experimental data are uncertain and therefore limit the accuracy of the calculations. Surface energy is a parameter that is known for being difficult to measure experimentally with accuracy. As a consequence coarsening processes are difficult to model with accuracy. Fortunately, new tools are available for calculating surface energies. Using ab initio calculations based on density functional theory surface and interfacial energies can now be calculated with a precision that is far better than experimental methods can offer. Results from such calculations will provide new and more reliable input data to programs like Thermo-Calc and DICTRA and will therefore contribute to more accurate modelling of materials behaviour in the future.

## Future prospects

Although DSS have been produced since the beginning of the 1930's new DSS emerge continually. The trend in alloy development has been to increase the concentrations of chromium, molybdenum and nitrogen so as to improve the resistance to pitting corrosion. Also copper has been added to some DSS to enhance the resistance to general corrosion. As with all remedies there are side-effects; Chromium and molybdenum both promote the formation of intermetallic phases while nitrogen is an ingredient in nitrides of the type  $\text{Cr}_2\text{N}$ . As a consequence, production is becoming increasingly difficult leading to intermetallic phase formation if the cooling rate is too slow and  $\text{Cr}_2\text{N}$  in the ferrite if it is too rapid. There is also evidence that copper promotes spinodal decomposition of ferrite [18]. It is, therefore, quite obvious that the laws of nature impose fundamental limits in alloy development. However, with more sophisticated production equipment the practical limits are continually pushed forward. As an example, recently developed DSS with a PRE-number close to 50 have been produced, thus confirming that alloys considered visionary a decade ago have now become a reality.

## Acknowledgements

This paper is published with permission from Sandvik Materials Technology. The support from Prof. Olle Wijk is gratefully acknowledged.

## References

- [1] H.D. SOLOMON and T.M. DEVINE, Proc. Conf. DSS (ed. R.A. Lula), Materials Park, OH, ASM, (1984) , pp. 693-756
- [2] J. CHARLES, Proc. Conf DSS '91, Les Ulis, France, Les Editions de Physique, (1991), pp. 3-48.
- [3] K. GÖRANSSON, M.-L. NYMAN, M. HOLMQUIST AND E. GOMES, Sandvik SAF 2707 HD, Internal lecture no. S-51-63, 2006.
- [4] N. JIA, R. Lin PENG, Y.D. WANG, G.C. CHAI, S. JOHANSSON, G. WANG, and P.K. LIAW, Acta Mater., 54, (2006), pp. 3907-3916.
- [5] G. CHAI and R. LILLBACKA, (2006), Key Engineering Materials 324-325, (2006), p. 1117.
- [6] R. LILLBACKA, G. CHAI, M. EKH, P. LIU, E. JOHNSON and K. RUNESSON, Acta Mater., 55, 2007, pp. 5359-5368.
- [7] P.R LIN, J. GIBMEIR, S. EULERT, S. JOHANSSON and G.C. CHAI, Materials Science Forum 524-525, (2006), p. 847.
- [8] G. HERBSLEB, Werkst. Korros., 33, (1982), pp. 33-34.
- [9] H. VANNEVIK, J.-O. NILSSON, J. FRODIGH and P. KANGAS, Trans. ISIJ 36, (1996), pp. 807-812.
- [10] P. KANGAS and J.-O. NILSSON, Proc. Stainless Steel World 05 Conf., Maastricht (2005), KCI Publishing BV, Zutphen, The Netherlands (2005).
- [11] A. TURNBULL, P.E. FRANCIS, M.P. RYAN, L.P. ORKNEY, A.J. GRIFFITHS AND B. HAWKINS, Corrosion 58 , (2002), p. 12.
- [12] S. SOLTANIEH, M. KLOCKARS, U. KIVISÄKK and P. EKLUND, Stainless Steel World 15, (2002), p. 28.
- [13] R. FRANCIS and G.R. WARBURTON, Proc. Stainless Steel World 99 Conf., Hague (1999), KCI Publishing BV, Zutphen, The Netherlands (1999), p.711
- [14] M. FERMENIA, J. PAN, and C. LEYGRAF, Journal of Electrochemistry Society 149, (2002) p. B187
- [15] M. FERMENIA, C. CANALISA, J. PAN, and C. LEYGRAF, Journal of Electrochemistry Society 150, (2003) p. B274.
- [16] B SUNDMAN, B. JANSSON and J-O ANDERSSON, Calphad, 9, (1985), pp 153-190
- [17] J-O. ANDERSSON and J. ÅGREN, J. Appl. Phys., 72, (1992), p. 153.
- [18] H.D. SOLOMON and L.M. LEVINSON, Acta Metal., 26, (1978), pp. 429-442.

# DETECTION OF THE 475°C EMBRITTLEMENT IN A LEAN DUPLEX STAINLESS STEEL USING THE ELECTROCHEMICAL POTENTIODYNAMIC REACTIVATION (EPR) TEST

*C. Fosca, J. Sakihama*

*Pontificia Universidad Católica del Perú, Peru*

## **Abstract**

The duplex stainless steel UNS S32101 (LDX 2101®) is a new leaner DSS that provide a high mechanical resistance with a corrosion behavior, in most cases, better than the traditional austenitic stainless steels. Although DSS are very competitive alloys, they are susceptible to precipitation of secondary phases as the spinodal decomposition of the ferrite, when they are exposed at temperatures between 300°-600°C. The  $\alpha$ - $\alpha'$  spinodal decomposition of ferrite can increase the hardness of the DSS but reduce strongly its toughness and corrosion resistance.

Microstructure changes for each aging condition were characterized by Electrochemical Potentiodynamic Reactivation EPR test in order to achieve a non destructive method to detect on service detrimental aging conditions in this alloy. The EPR test was carried out using an appropriate electrolyte composition (H<sub>2</sub>SO<sub>4</sub> with addition of KSCN) at 20°C. The reactivation potential and scan rate were selected to improve more sensitivity to the microstructural changes.

## **Introduction**

LDX 2101® (EN 1.4162, UNS S32101) is a new low alloyed (lean) Duplex Stainless Steels with low addition of nickel in order to reduce the cost. To assure an adequate phase balance in the microstructure (50% austenite, 50% ferrite), the austenite stability effect of the nickel is replaced with additions of manganese and nitrogen. The mechanical resistance of this alloy is comparable with the DSS 22%Cr-5%Ni (EN 1.4462, UNS S32205) and the corrosion properties are in general better than for austenitic 304 (EN 1.4301)

The unique combination of mechanical properties, corrosion resistance and low cost, make this alloy an excellent choice for many applications for which the traditional austenitic stainless steel are usually employed.

Its relative low alloy content in comparison with others DSS brings the additional advantage to be less sensitive to the secondary phase precipitation, when these materials are heated in the range of 700°- 900°C (sigma phase, Chi-, R- phases, carbides) and in the range of 300° - 600°C ( $\alpha$ - $\alpha'$  spinodal decomposition of ferrite). All of these phase precipitations produces a strong reduction of the material toughness, known as thermal aging embrittlement of DSS.

Many researches have investigated and developed different methods to detect and also to quantify the thermal embrittlement in the DSS [1,2,3,4]. Due to the presence of precipitated phases promoted not only the embrittlement but also the localized corrosion of the DSS, electrochemical techniques can be used to detect microstructural changes in these alloys [5].

The Electrochemical Potentiodynamic Reactivation (EPR) test, originally developed to detect the intergranular corrosion of austenitic stainless steel, has been used also to detect the susceptibility to intergranular corrosion of DSS due secondary phases [6,7,8] but there are scarce published results about the use of this electrochemical technique to detect the 475°C embrittlement of DSS [9]. The aim of this article is to study the use of the EPR technique on the detection of the  $\alpha$ - $\alpha'$  aging embrittlement in a new lean duplex stainless steel.

## Experimental Procedure

As mentioned before, the material studied was the LDX 2101® duplex stainless steel. The alloy was supplied in the form of a 6 mm plate in as received condition, with a chemical composition described in table 1. The samples were aged at  $475 \pm 5^\circ\text{C}$  during different times (4, 8, 16, 24, 48 and 72hrs) and cooled with water at room temperature.

Table 1. Chemical composition of the LDX 2101® duplex stainless steel.

C	Si	S	P	Mn	Ni	Cr	Mo	V	Cu
0.035	0.73	0.002	0.002	4.87	1.52	21.83	0.28	0.05	0.32
W	Ti	Sn	Co	Al	B	Nb	N	Fe	
0.015	0.01	0.005	0.043	0.023	0.002	0.008	0.22	rest	

## Mechanical testing

Hardness measurements and impact testing were carried out in the aged samples in order to study the effect of the aging time at 475°C on the mechanical properties. Vickers Hardness measurements were made on 10mm x 10mm area specimen with a 20Kg load. Charpy Impact test were conducted at 0°C using three specimens for each aging time condition. Because the thickness of the plate, 6x10x55 mm<sup>3</sup> reduced charpy - V notch samples were used as shown in figure 1.

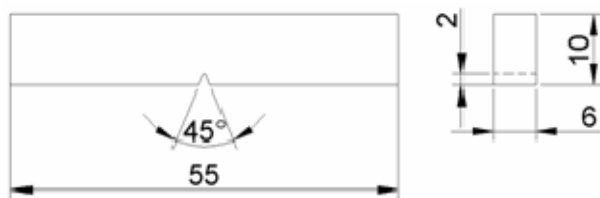


Figure 1. Reduced Charpy V-notched samples used in the impact testing

## Microstructural analysis

The determination of ferrite content was done on a Fisher Ferritescope® MP30E working according to DIN 32514-1. For the metallographic analysis the samples were mounted in resin, grinded, polished and etched using the Bloech and Wedl color etching agent.

## Electrochemical Potentiodynamic Reactivation (EPR) testing

A modified Double loop Electrochemical Potentiodynamic Reactivation (DL-EPR) test was used to detect possible different reactivation grades as consequence of the aging level at 475°C. The samples were mounted in resin and polished. They were submerged with an exposed area of 24 mm<sup>2</sup> in a 50 ml glass beaker together with a Pt counter electrode, saturated calomel reference electrode was submerged in a 3.5M KCl solution and was connected with a salt bridge to the electrolyte solution (figure 2). The electrolyte composition was optimized to obtain the higher sensitivity of the test for this alloy in the studied conditions. The electrolyte solution was 0.5M H<sub>2</sub>SO<sub>4</sub> with 0.01M KSCN, The solution temperature was maintained at 20°C. Before scanning a preconditioning of the surface was carried out at -700 mV (SCE) during 60 seconds with a stabilization time at corrosion potential for another 60 seconds. The potential was scanned from the corrosion potential (open circuit potential) to +200 mV (SCE) and immediately the scan is reversed to reach again the corrosion potential. The scan rate for both scan directions was 2 mV/s.

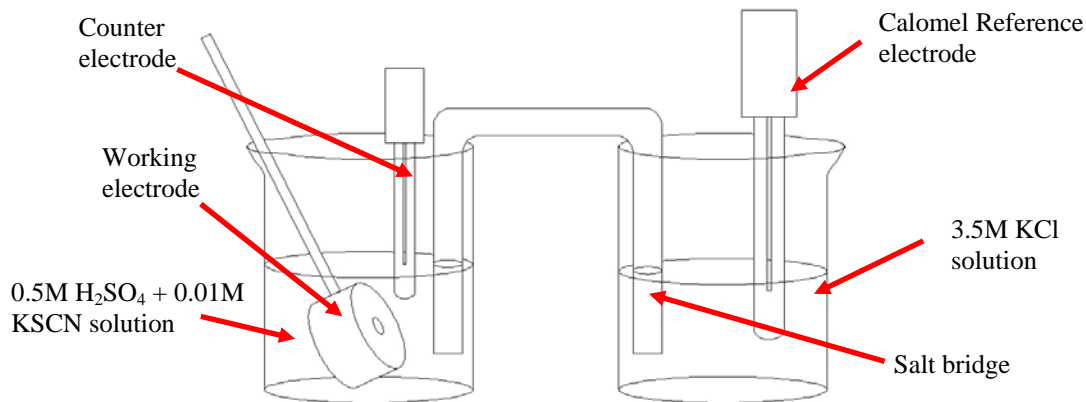


Figure 2. Corrosion cell used for EPR tests.

The sensitization grade is determined by the ratio of the reactivation current ( $I_r$ ) and the activation current ( $I_a$ ), using the  $I_r/I_a$  ratio as a measure of the degree of sensitization (figure 3).

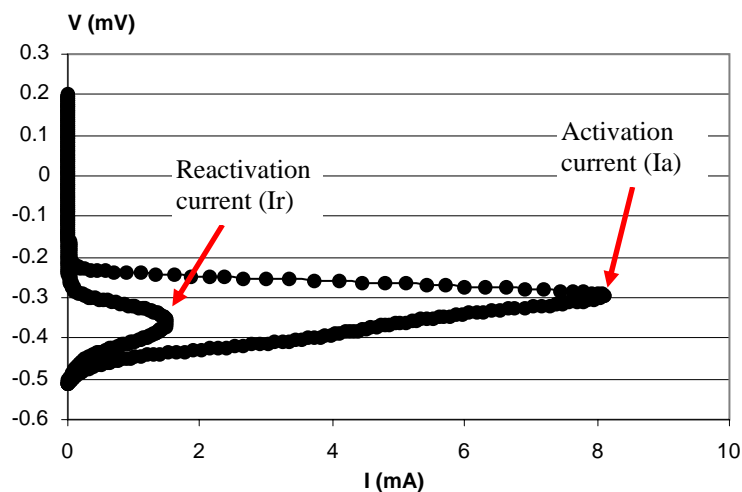


Figure 3. Typical DL-EPR curve.

## Results and Discussion

### Mechanical properties

The aging at 475°C of the LDX 2101® duplex stainless steel produced only a slight increase in hardness, observed in the first 4 hours of aging. However the impact test results confirmed the embrittlement effect of the aging treatments. The toughness decreased in about 40% after 72 hours at 475°C.

A first conclusion from these results is the poor correlation between the hardness values and impact test results, hardness measures should not be used to detect the embrittlement effect of the aging condition.

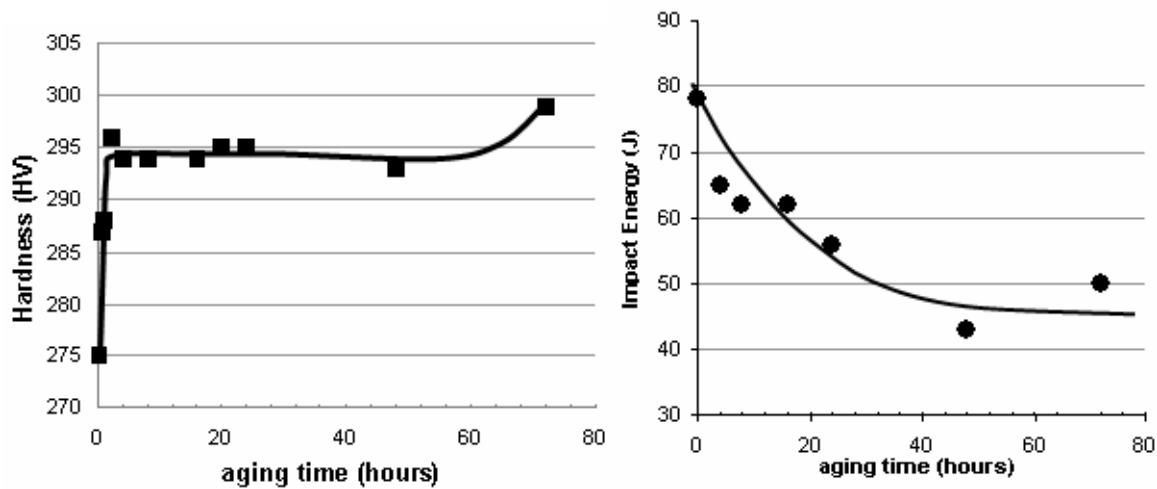


Figure 4. Hardness measurements and Impact energy (at 0°C) vs aging time at 475°C for the LDX 2101® duplex stainless steel.

### Microstructural analysis

The ferrite volume fraction suffers a slight decrease after the aging, as shown in figure 4, from 52.2% to 42.6% after 72 hours, observing the strongest variation during the first 4 hours aging treatment (figure 4). After this time the aged alloy shows stabilization on the % ferrite content for longer aging periods.

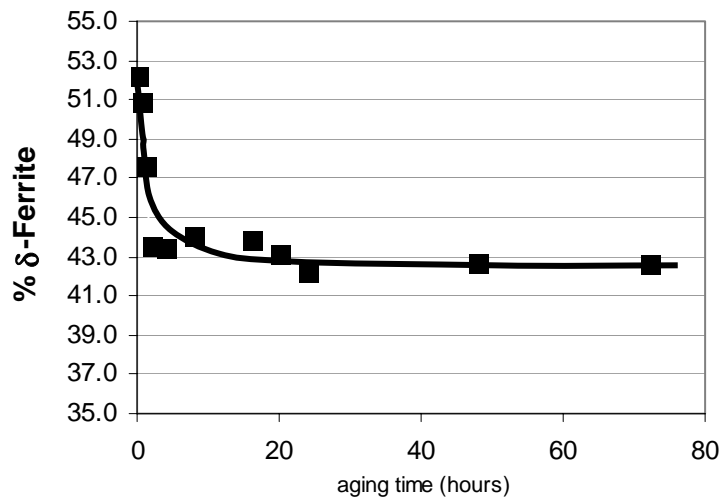
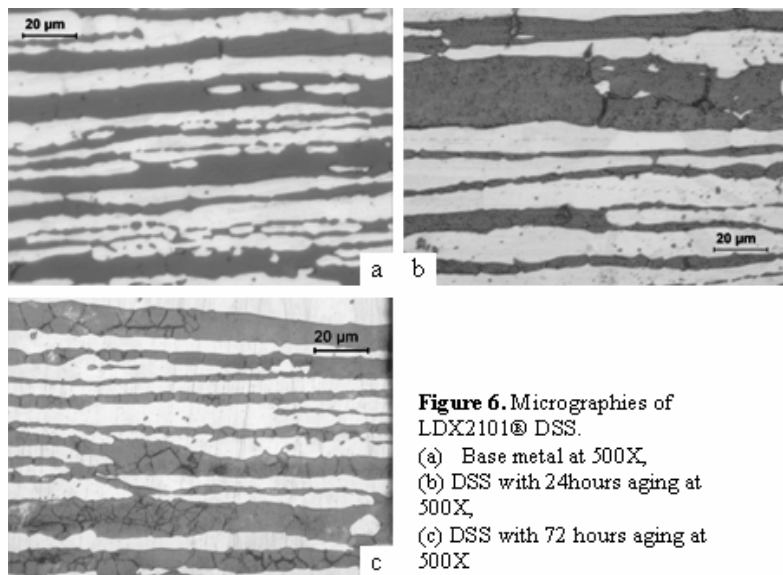


Figure 5.  $\delta$ -Ferrite percentage measured by magnetic induction measurement method vs. aging time.

Observing the figures 4 and 5 it finds a good correlation between the hardness variation and the ferrite content in the microstructure for the aged samples. However, neither the hardness measurement nor the ferrite content determination can be used as indirect method to detect 475°C-embrittlement in this alloy because the measured values fall within the typical ranges observed in normal microstructural conditions, where there is no embrittlement problem.

The metallographic analysis by optical microscopy using color etching showed clear differences in the microstructure for the aged samples. Figure 6a shows the microstructure of the DSS basis material, where the dark phase is ferrite and the light phase is austenite. Figures 6b and 6c show indications in ferrite phase after 24 and 72 hours aging heat treatment

The observation of microstructural changes by optical microscopy for low aging temperatures in DSS is very difficult. Commonly the evidence of a possible spinodal decomposition of ferrite can be obtained observing the microstructure by TEM [3] because the size of Cr-rich  $\alpha'$  precipitates is about a few nanometers. The color etching method, used in this study, can detect difference between the micrographies for the 475°C aging conditions by optical metallography. The optical micrographies do not revealed directly the  $\alpha'$  precipitates but yes its effect on the interference film, formed during the color etching on the surface of the metallographic sample. These micrographic differences were evident from 24 hours aging treatment (figure 6.b).



### EPR testing

Figure 7 shows the results of the double loop EPR tests, in function of the coefficient  $I_r/I_a$  versus aging time at 475°C. Here we can observe an increase of the sensitization, due presumably to the precipitation of Cr-rich  $\alpha'$  phase into the ferrite and the resultant depletion of Cr around it.

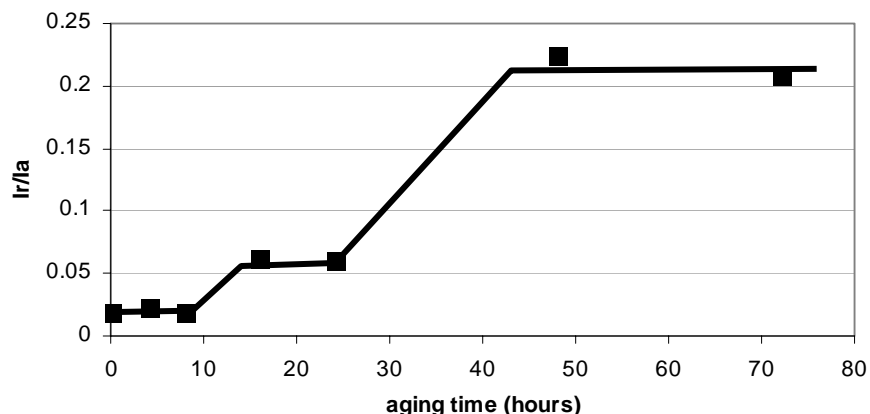


Figure 7. Sensitization by DL-EPR test ( $I_r/I_a$ ) vs aging time at 475°C

There is a slightly similar tendency between the impact toughness results (figure 4) and the  $I_r/I_a$  ratio obtained by EPR test (figure 7) in the studied aging conditions. The decrease in impact energy of the aged alloys is consequence of the diminution of the dislocation mobility due to  $\alpha'$ -ferrite precipitation. On the other hand, the sensitization index is related to the degree of the Cr depletion around this precipitates. In the studied conditions, both mechanisms probably have been rising with the aging time.

## Conclusions

- DSS LDX 2101®, suffers 475°C - aging embrittlement, reducing its toughness after 72 hours about 40% of its as received condition.
- Bloech and Wedl Color etching allowed to identify micrographies associated to aging conditions in the DSS.
- The Ir/Ia ratio of DL-EPR test was found to be a good measure of the degree of 475°C embrittlement in the studied aging conditions due to its good correlation with the impact test results.

## Acknowledgments

The authors are grateful to Outokumpu S.A. (Barcelona) for supplying the duplex stainless steel.

## References

- [1] EVANSON, S.; OTAKA, M.; HASEGAWA, K. "Use of Squid Magnetic Sensor to Detect Aging Effects in Duplex Stainless Steel" *British Journal of Non-Destructive Testing*, Vol. 32, No. 5, 1990, pp. 238-240
- [2] Y ISHIKAWA, M OHTAKA, S TSUCHIYA, T YOSHIMURA, "Atom-probe study of the aging embrittlement of cast duplex stainless steel". *SME International Journal Series A*, Vol. 38, p. 384,1995.
- [3] S.S.M. TAVARESA, R.F. DE NORONHA, M.R. DA SILVA, J.M. NETO, S. PAIRIS "475°C Embrittlement in a Duplex Stainless Steel UNS S31803" *Materials Research*, Vol. 4, No. 4, 237-240, 2001.
- [4] H. OGI, M. HIRAO "Ultrasonic Noise Relaxation for Evaluating Thermal Aging Embrittlement of Duplex Stainless Steels". *Research in Nondestructive Evaluation*, Vol. 9, No. 3, November 1997.
- [5] CHAN-JIN PARK, HYUK-SANG KWON. „Electrochemical noise analysis of localized corrosion of duplex stainless steel aged at 475°C". *Materials Chemistry and Physics* 91 (2005) 355–360.
- [6] C. Fosca. "Influencia de la fase sigma sobre la resistencia a la corrosión por picaduras de aceros inoxidables duplex y su caracterización electroquímica mediante la técnica EPR" tesis doctoral, Universidad Complutense de Madrid, España. 1995.
- [7] T. AMADOU, C. BRAHAM, and H. SIDHOM. "Double Loop Electrochemical Potentiokinetic Reactivation Test Optimization in Checking of Duplex Stainless Steel Intergranular Corrosion Susceptibility". *Metallurgical and Materials Transactions A* Volume 35A, November 2004. 3499-3513.
- [8] C.J. PARK, V. SHANKAR RAO, AND H.S. KWON. "Effects of Sigma Phase on the Initiation and Propagation of Pitting Corrosion of Duplex Stainless Steel" *Corrosion*, Vol. 61, No. 1, 2005, 76-83.
- [9] CHAN-JIN PARK, HYUK-SANG KWON. "Effects of aging at 475°C on corrosion properties of tungsten-containing duplex stainless steels" *Corrosion Science*, 44 (2002) 2817–2830.



# MILL EXPOSURE TESTS OF DUPLEX STAINLESS STEEL LDX 2101<sup>®</sup> IN RECYCLED FIBER APPLICATIONS

*T. Laitinen<sup>1</sup>, L. Wegrelius<sup>2</sup>, A. Bergquist<sup>2</sup>*

*<sup>1</sup>Metso Paper, Finland, <sup>2</sup>Outokumpu Stainless AB, Sweden*

## **Abstract**

The performance of a newly developed duplex stainless steel LDX 2101<sup>®</sup> (EN 1.4162) was compared with traditional construction material, in the first place EN 1.4432 (316L). Test coupons were exposed in recycled fiber (RCF) mill environments while erosion corrosion tests were performed in the laboratory.

RCF mill tests were performed in Scandinavia, Europe and Asia. Test coupons were installed in the liquid phase inside pulpers and other RCF line equipment for 2 – 7 months. The RCF mill environment can contain large amounts of abrasive particles like sand, metal, glass and plastic. Erosion corrosion tests were performed in laboratory environments containing chloride- and sulphate ions or in sulphuric acid loaded with 100 g/l silica sand at a temperature of 50°C.

The in-plant tests showed that in mild RCF environment, with chloride levels below 150 mg/l, no measurable difference regarding corrosion performance existed between the tested steel grades LDX 2101<sup>®</sup> and 1.4432. On the other hand, in more aggressive environments, grade 1.4432 was slightly more corrosion resistant. In the erosion corrosion tests, grade LDX 2101<sup>®</sup> performed best in all tested environment/load combinations. The results were expected considering, that 1.4432 is slightly more corrosion resistant in acidic and near neutral solutions containing chlorides, while LDX 2101<sup>®</sup> is more wear resistant.

## **Introduction**

Recycled pulp is made from paper and board, which has been used and then recovered, by one of various waste collection schemes. Waste paper contains impurities of various kinds, e.g. plastics, metals, printing ink and netting spines from books, which cause a more abrasive condition than in other kind of pulping processes.

The austenitic stainless steel grade 1.4432 has so far been the dominating construction material for equipment in RCF processes. However, duplex stainless steels are becoming more and more frequently used in many applications, including pulp and paper processes. The mechanical strength of duplex stainless steels is approximately twice as high as for conventional austenitic grades, implying not only benefits in terms of reduced gauges and reduced weight, but also a higher resistance towards abrasive conditions.

LDX 2101<sup>®</sup> is the latest contribution in the duplex stainless steel family with the same desirable properties as other duplex stainless steels - good corrosion resistance, welding and engineering properties. LDX 2101<sup>®</sup> has a low nickel content that implies a low and stable price and together with the high strength it is a cost efficient alternative to the more traditional austenitic stainless

steel grades. The purpose of this investigation was to study the performance of LDX 2101<sup>®</sup> in recycled fiber processes.

## Experimental

### Test materials

Table 1 shows the typical composition, the pitting resistance equivalence (PRE = %Cr + 3.3x%Mo + 16x%N) and proof strength of the investigated stainless steel grades.

Table 1. Typical composition in weight %, PRE values and proof strength of investigated stainless steel grades.

Grade	EN	ASTM	C	Mn	Cr	Ni	Mo	N	PRE	R <sub>p0.2</sub> *
LDX 2101 <sup>®</sup>	1.4162	S32101	0.03	5	21.5	1.5	0.3	0.22	26	450
4301	1.4301	304	0.04	-	18.1	8.1	-	0.05	19	210
4404	1.4404	316L	0.02	-	17.2	10.1	2.1	0.05	25	220
4432	1.4432	316L	0.02	-	16.9	10.7	2.6	0.05	26	220

\* Hot rolled plate, min values at 20 °C according to EN 10088.

LDX 2101<sup>®</sup> is a registered trade name by Outokumpu.

### Mill exposure tests

The test coupons, for the mill exposures, were water-cut from hot rolled plate, measuring 60 x 60 x 8 mm. The coupons had mill surface finish (hot rolled, heat treated and pickled) and the cut edges were dry-ground to 320 grit. The coupons were mounted on an insulated bolt with flat polytetrafluoroethylene (PTFE) crevice washers separating the coupons from the test rack. Each test rack contained three coupons in the same steel grade bolted to a plate made of the stainless steel grade 2205. The bolts were assembled to the rack using a torque of 4 Nm. The test rack assembly is illustrated in Figure 1.



Figure 1. Test rack for mill exposure and coupon assembly.

Before the exposure the coupons were weighed, the dimensions measured and the surface roughness characterized by Optical Confocal Microscopy. After the exposure each rack was dismantled, the coupons brushed under running water and cleaned in 20% nitric acid solution at room temperature for at least 15 minutes and dried. After cleaning the coupons were weighed, the surface roughness (Ra) was measured, and they were examined in a binocular at 20X magnification. The mill exposure tests were performed in several RCF mills in Scandinavia (4 mills), Europe (2 mills) and Asia (1 mill). The test coupons were installed inside the pulping line equipment and were thus exposed in liquid or in liquid + gas environments. The process equipments are specified in Table 2 and the process environment is given in Table 3. Pulp made of old corrugated cardboard (OCC-pulp) is typically not bleached, as was the case with all the OCC lines in this study. De-inked pulp (DIP) is usually bleached with H<sub>2</sub>O<sub>2</sub>, dithionite (hydrosulphite), formamidine sulphinic acid (FAS) or their combination. In Mill A, DIP was bleached with H<sub>2</sub>O<sub>2</sub>, in Mill B with H<sub>2</sub>O<sub>2</sub> and FAS and in Mill G with H<sub>2</sub>O<sub>2</sub>. Samples of the process environment were taken from the test sites and analyzed by Dionex ion chromatography

system equipped with an AS50 autosampler, a LC25 chromatography oven, an EG40 eluent generator, and an IC25 ion chromatograph. The required concentration for the mobile phase (potassium hydroxide) was made simultaneously in the eluent generator module by using the Dionex EGC II KOH cartridge. The samples were processed with conservatives due to several days delay to the analysis. [1]

Table 2. Exposure test conditions.

Test site	Location	RCF pulp	Fresh water [m <sup>3</sup> /t pulp]	Equipment	Bleaching	Environment
Mill A	Scandinavia	DIP	30	HC pulper	H <sub>2</sub> O <sub>2</sub>	Liquid + gas
Mill B	Scandinavia	DIP	30	GapWasher	FAS and H <sub>2</sub> O <sub>2</sub>	Liquid + gas
Mill C	Scandinavia	OCC	20	Drum pulper	None	Liquid + gas
Mill D	Scandinavia	OCC	Not known	Fine screen Support structure	None	Liquid
Mill E	Europe	OCC	1,3	Coarse screen	None	Liquid
Mill F	Europe	OCC	6	LC pulper	None	Liquid + gas
Mill G	Asia	DIP	15 - 20	Drum pulper	H <sub>2</sub> O <sub>2</sub>	Liquid + gas

Pulpers are used for disintegrating the raw material (pulp bale, recycled paper, broke from paper machines) into a form ready for pumping. Pulpers operate either in low consistency (LC) or in high consistency (HC). Drum pulpers also remove large impurity particles and ink from recycled paper. GapWashers are used for washing ash, ink and stickies from pulp and for pulp thickening up to 10%. Screens are used to separate fibers by fiber length.

Table 3 The chemistry of the media at the different test sites.

Test site	Exposure time [months]	Temp [°C]	pH	Cl <sup>-</sup> [mg/l]	SO <sub>4</sub> <sup>2-</sup> [mg/l]	SO <sub>3</sub> <sup>2-</sup> [mg/l]	S <sub>2</sub> O <sub>3</sub> <sup>2-</sup> [mg/l]	Molar ratio [Cl <sup>-</sup> ]/[SO <sub>4</sub> <sup>2-</sup> ]	Molar ratio ((Cl <sup>-</sup> )+[SO <sub>4</sub> <sup>2-</sup> ])/[S <sub>2</sub> O <sub>3</sub> <sup>2-</sup> ]
Mill A	2, 4, 6.5	37.8	7.2	37	523	NA	1	0,19	730
Mill B	2, 4, 6.5	48.7	6.9	114	703	4	1	0,44	1200
Mill C	2, 4, 6.5	48.8	7.1	80	945	163	305	0,23	4,4
Mill D	6 ?	NA	NA	322	100	10	2	8,7	570
Mill E	7	NA	NA	787	1243	0	21	1,7	192
Mill F	4	NA	NA	861	625	0	0	3,7	-
Mill G	-	NA	NA	165	193	29	2	2,3	350

NA – not analysed.

### Laboratory erosion corrosion tests

Cylindrical test samples, in grade 1.4301 and 1.4404, were prepared from Ø 12 mm bar by turning to a diameter of 8 mm. Test samples, in grade 1.4432 and LDX 2101<sup>®</sup>, were prepared by cutting cylindrical Ø 8 mm samples from 10 mm thick plate. The cylindrical samples were ground with 180 grit paper, cleaned with ethanol and dried. The sample area was measured in 1 mm<sup>2</sup> accuracy and sample weight in 0,1 mg accuracy. Erosion corrosion tests were executed in a decanting tank, where rotation speed of the horizontal agitator was 425 rpm. Test samples were attached on the rim of the decanting tank and exposed to the test environment for 5 to 24 h. The erosion corrosion test environments contained either chloride together with sulphate or plain sulphuric acid. Silica sand was used as the wearing agent. The test environments are presented in Table 4.

Table 4. Erosion corrosion test environments.

	Cl <sup>-</sup> [mg/l]	SO <sub>4</sub> <sup>2-</sup> [mg/l]	Molar ratio [Cl <sup>-</sup> ]/[SO <sub>4</sub> <sup>2-</sup> ]	H <sub>2</sub> SO <sub>4</sub> [g/l]	Silica sand [mg/l]	pH	Temp [°C]	Immersion [h]	Wearing [h]
Test1Env1	200	542	1	-	100	5	50	0	24
Test1Env2	1000	2708	1	-	100	5	50	0	24
Test2Env1	200	542	1	-	100	5	50	168	5
Test2Env2	1000	2708	1	-	100	5	50	168	5
Test3Env3	-	-	-	49	100	~ 0	50	0	5

## Results

### Mill exposure tests

The process environments of the mill sites are presented in Table 3. Mills A, B, C and D were in Scandinavia, Mills E and F in Europe and Mill G in Asia. H<sub>2</sub>O<sub>2</sub> bleaching residues of the process samples were not analyzed because H<sub>2</sub>O<sub>2</sub> residues do not stand the preservation process. The European mills E and F had high chloride (Cl<sup>-</sup>) contents due to a low fresh water supply (< 6 m<sup>3</sup>/t pulp). The sulphate (SO<sub>4</sub><sup>2-</sup>) level was exceptionally low in the Scandinavian mill D and in the Asian mill G, which has been the case with several other Asian mills. The reason for the low sulphate concentration might be the raw material.

Remarkable high sulphite (SO<sub>3</sub><sup>2-</sup>) and thiosulphate (S<sub>2</sub>O<sub>3</sub><sup>2-</sup>) concentrations were determined at mill C, where no bleaching was used. The reason for this high thiosulphate concentration was suspected to be remnants from the pulp cooking.

Table 5 shows the summary of the test results from the mill exposures. Especially at mill A and mill F, some weight loss was measured, which most certainly was due to mechanical impacts. The mechanical load on the test coupons was really heavy indicated by the fact that, at mill F only one coupon of grade 1.4432 remained after the test period and at mill G all the test coupons had fallen off the test test racks and disappeared in the process. The weight loss was maximum 226.5 mg for grade LDX 2101<sup>®</sup> (at mill A) and 646.6 mg for grade 1.4432 (at mill F), corresponding to a maximum corrosion rate of 0.011 mm/year and 0.025 mm/year respectively. A material with a corrosion rate below 0.1 mm/year is normally considered as corrosion proof.

Table 5. Summary of the mill exposure test results after approximately 2, 4 and 6.5 months exposure.

Test site	Steel grade	Corrosion rate [mm/y]			Remarks
		2 month	4 month	6.5 month	
Mill A	LDX 2101 <sup>®</sup>	0.016	0.009	0.011	No local corrosion, minor mechanical marks
	1.4432	0.012	0.006	0.008	No local corrosion, minor mechanical marks
Mill B	LDX 2101 <sup>®</sup>	0.000	0.000	0.000	No local corrosion
	1.4432	0.001	0.001	0.000	No local corrosion, minor mechanical marks
Mill C	LDX 2101 <sup>®</sup>	0.000	0.000	0.000	No local corrosion, some weld sputter on the coupons
	1.4432	0.000	0.001	0.001	No local corrosion, some weld sputter on the coupons
Mill D	LDX 2101 <sup>®</sup>			-	Localized corrosion, max Ø 200 µm, crevice corrosion under deposits (2 screen support rods for 7 months)
Mill E	LDX 2101 <sup>®</sup>	-	-	-	No local corrosion, minor mechanical marks, 3 coupons for 7 months
	1.4432	-	-	-	No local corrosion, minor mechanical marks, 3 coupons for 7 months
Mill F	LDX 2101 <sup>®</sup>	-	-	-	Lost during exposure
	1.4432	-	0.025	-	No local corrosion, mechanical damage. 2 and 6.5 month coupons lost during exposure
Mill G	LDX 2101 <sup>®</sup>	-	-	-	All coupons lost during 24 months exposure
	1.4432	-	-	-	All coupons lost during 24 months exposure

## Laboratory erosion corrosion tests

Erosion corrosion tests were performed in three different test solutions with or without an immersion period followed by a wearing cycle. Duplicate test samples were used in all tests. In the 24 h erosion corrosion test cycle (Test1) without any immersion pre-treatment, all the tested materials remained passive and the weight losses obtained were due to wearing purely. However, when the test materials were pre-treated by immersion for one week in the high-chloride test solution (1000 mg/l) followed by 5 h wearing (Test2Env2), the passive film broke down locally, resulting in both some pitting and wearing. In the 1 N H<sub>2</sub>SO<sub>4</sub> solution all the test materials corroded actively and wearing took place very rapidly during the 5 h wearing cycle (Test3Env3), corresponding to a erosion corrosion rate of about 1 mm/year. The results are presented in Figure 2.

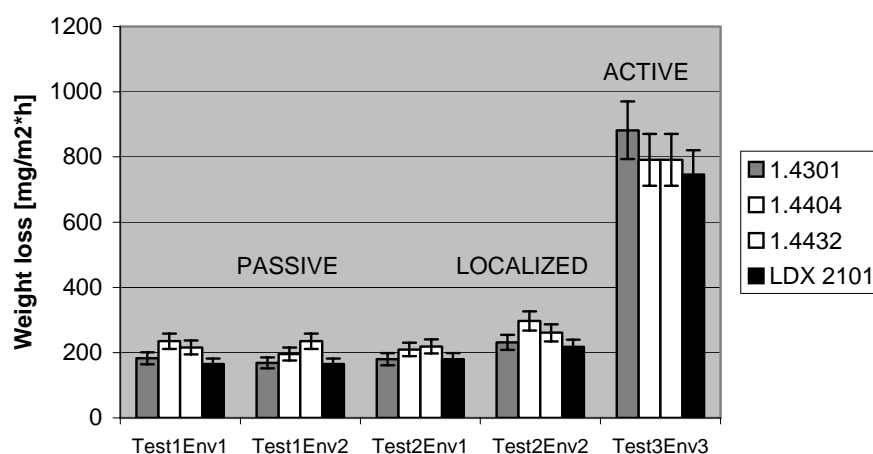


Figure 2. Erosion corrosion test results presented as a function of weight loss [mg/m<sup>2</sup>\*h].

The erosion corrosion rate of 1.4432 was 24 – 30% higher than the erosion corrosion rate of LDX 2101<sup>®</sup> in the mildest environment containing 200 mg/l chloride (Env1). In 1000 mg/l chloride (Env2) containing environment the erosion corrosion rate difference was 16 – 18%. In the most aggressive environment (Env3) the erosion corrosion rate of 1.4432 was only 6% higher than the rate of LDX 2101<sup>®</sup>.

## Discussion

Sulphate ions are known for inhibiting the pitting corrosion of stainless steel in chloride containing media. The inhibitive effect of sulphate ions on the initiation of pitting, has been proposed to be based on the competitive adsorption with chloride ions [2]. So, with high chloride- and low sulphate levels, the molar ratio [Cl<sup>-</sup>]/[SO<sub>4</sub><sup>2-</sup>] becomes high, which in turn increases the risk of pitting and crevice corrosion. This is also indicated in the result of this study, mill D having the highest chloride to sulphate ratio, was the only mill showing signs of corrosion. In mills A, B, C and E having low chloride to sulphate ratios, there were no signs of corrosion on any of the investigated steel grades.

Experience from the paper industry has shown that traces of thiosulphate can cause pitting on stainless steel grade 1.4301 (304) in what otherwise is rather benign and non-corrosive white water. Thiosulphate comes mainly from the hydrosulphite brightening, as a decomposition product, in the papermaking process. The most sensitive concentration range has been found to be when the molar ratio  $([Cl^-] + [SO_4^{2-}]) / [S_2O_3^{2-}]$  is in the order of 10 to 30 [3]. The result from this study does neither confirm nor reject the theory of this corrosion sensitive molar ratio. Most

of the mills had a molar ratio far above 30, only mill C had a ratio close to the sensitive area. However, there was no corrosion at all in mill C.

Except from some minor pitting and crevice corrosion attacks on LDX 2101<sup>®</sup> at mill D, having the highest chloride to sulphate ratio, no measurable difference regarding corrosion resistance could be detected between the tested grades LDX 2101<sup>®</sup> and 1.4432. From corrosion point of view, recycled pulp is not a very aggressive environment. On the other hand, the recycled fibre contains a lot of abrasive impurities, e.g. plastics, paper-clip, staples, netting spines from books, which cause an abrasive condition. The fact that most of the coupons were lost at mill F and G is an indication of that the mechanical forces during the processing of the recycled pulp are high. In the absence of corrosion, the mechanical abrasion of the coupons was, especially for grade 1.4432, the most predominating feature. That is also supported by the fact that the surface roughness for grade 1.4432 increased slightly after exposure at the test sites. The laboratory erosion corrosion tests show that the mechanical strength of the material has a big impact on the overall performance as grade LDX 2101<sup>®</sup> experienced the lowest weight losses in all test environments.

Duplex stainless steels are more and more taking over the role of austenitic stainless steels like 1.4301 and 1.4432 in papermaking equipments. Nitrogen as an alloy addition makes the duplex steels more pitting resistant and stronger. They also have the added advantage of resisting stress corrosion cracking that can occur on higher temperature components such as steam boxes.

## Conclusions

The result from the exposure at the mills and the erosion corrosion tests shows that:

- The duplex stainless steel grade LDX 2101<sup>®</sup> can in most situations replace the conventional austenitic grade 1.4432 in recycled fibre applications.
- Some cautions should however be taken when the chloride level of the process water becomes high.
- The high strength of LDX 2101<sup>®</sup> gives an extra advantage of high resistance under abrasive conditions.

## References

- [1] J.P. Isoaho, personal communication 2007.
- [2] H.P. Leckie: 'Environmental Factors Affecting the Critical Potential for Pitting in 18-8 Stainless Steels', J.Electrochem. Soc. 113, 12, 1966, pp. 1262 – 1267.
- [3] R.C. Newman, W.P. Wong, H. Ezuber and A. Garner: 'Pitting of stainless steel by thiosulfate ions', Corrosion 45 , 4, 1989, pp. 282 – 287.

# A NEW LEAN DUPLEX STAINLESS STEEL WITH HIGH MECHANICAL AND CORROSION PROPERTIES: 1.4062

*J. Peultier<sup>1</sup>, E. Chauveau<sup>2</sup>, S. Jacques<sup>1</sup>, M. Mantel<sup>2</sup>*

*<sup>1</sup>Industeel (ArcelorMittal group), France, <sup>2</sup>Ugitech (Schmolz + Bickenbach group), France*

## Abstract

Due to low Ni content, the price of duplex family is less sensitive to the price fluctuation of raw materials than the price of austenitic family. In numerous applications, a very cost effective duplex solution can nowadays be proposed as an alternative to austenitic material with at least a similar corrosion resistance and better mechanical properties. For instance, 1.4362 (UNS S32304) replaced 1.4404 (316L) material in evaporators of sea water desalination units or in pumps and valves for process and water industries; 1.4462 (UNS S32205) is used instead of 1.4439 (317LMN) in the absorbers of wet flue gas desulphurization systems.

This paper presents a new lean duplex grade developed in close cooperation between Industeel and Ugitech with the aim to propose a cost effective alternative to 1.4307 (304L), coated or galvanized carbon steel or concrete in structural applications, potable water systems or pulp and paper industry. The reduction of Ni is obtained by a nitrogen addition in order to obtain microstructure containing approximately 50% of ferrite and 50% of austenite. After a preliminary study performed with laboratory heats, several industrial heats were produced with 22Cr%, 2Ni% and 0.2%N as typical composition.

In this paper, the results of investigation performed on industrial bars, cold-drawn wires and hot rolled plates are presented and discussed. It appears that this new lean duplex grade (UNS S32202 / EN 1.4062) has a localized and uniform corrosion better than 1.4307 material with yield strength about twice.

## Introduction

Austenitic stainless steels, such as 1.4301 (18Cr8Ni) and 1.4401 (17Cr10Ni2Mo) types account for 60% of stainless steels usage all over the world. This is certainly the result of their corrosion resistance properties but also of their versatility and ease of fabrication. Their major drawbacks are their low mechanical strength and their exposure to alloy cost variations.

While ferritic grades (17Cr, 17CrTi) have found increasing applications in thinner gauges, they cannot easily replace austenitics in thicknesses over 3mm, due to their inherent tendency to grain coarsening (especially in heat affected zone of welds). Furthermore, 200 series Mn grades are limited to very low corrosive media due to their relatively low Cr content.

In the duplex family and thanks to progress made in steel metallurgy since 70's, 1.4462 (2205) is now recognized as a cost effective and technically efficient solution<sup>1</sup>. For instance, 1.4462 replaced 1.4439 (317LMN) in air pollution control equipment<sup>2</sup> and 1.4429 (316LN) or 1.4404 (316L) in chemical tankers<sup>3</sup>. Although 1.4362 (2304) was developed over 20 years ago, it never

succeeded in challenging the supremacy of 1.4462 in period where the price of Ni and Mo remained under control. But, present raw materials prices have increased the price gap between austenitics and duplex. Consequently, Mo free 1.4362 grade constitutes at that time an excellent cost alternative to the austenitic 1.4404 solution, explaining 1.4362's growth acceleration since 2003, as for instance in desalination industry<sup>4</sup>, marine applications or production process<sup>5</sup>.

The new lean duplex grade 1.4062 (UNS S32202), presented in this paper, was developed to match the corrosion resistance of 1.4301 or 1.4307 austenitic grades in most environment and with twice mechanical strength. The nominal chemical composition of this grade is 22Cr%, 2Ni% and 0.2%N with iron balance. It was designed not only to obtain mechanical properties and corrosion resistance, but also structural stability and good toughness properties in the heat affected zone of welded assemblies. The Cr content, element which is known to be beneficial in fighting against all the corrosion forms, was kept higher than 21.5%. Ni content was optimized to obtain crevice corrosion resistance and toughness properties without increasing the material price. N content was adjusted to obtain a microstructure containing approximately equal amounts of ferrite and austenite after an annealing treatment performed in the range 980 – 1100°C. This grade is Mo free to offer better structural and cost stabilities. Finally Mn was kept below 2% in order to limit its detrimental effect on pitting corrosion resistance, due to the formation of manganese sulphides or manganese oxisulphides, but also on uniform corrosion resistance in sulphuric acid solution<sup>6</sup>. After a first test program with laboratory heats of 25kg, several industrial heats were produced in Industeel and Ugitech melting shops, then transformed in plates, bars, rebars or cold drawn wires. This paper presents the mechanical and corrosion properties obtained on these industrial products. Compositions of tested materials including the reference austenitic and duplex grades are given in Table 1.

Table 1. Typical chemical composition and PREN value for tested stainless steels (PREN = Cr% +3.3Mo% +16N%)

Euronorm	AISI	C	Cr	Ni	Mo	N	Others	PREN
1.4301	304	< 0.070	18.5	9				18.5
1.4307	304L	< 0.030	18.5	10.5				18.5
1.4404	316L	< 0.030	17	11.5	2.1			24
1.4571	316Ti	< 0.080	17	11	2.1		Ti <sub>≥</sub> 5(C+N)	24
1.4429	316LN	< 0.030	17.5	11.5	2.6	0.15		29
1.4062	2202	< 0.030	22.5	2	0.3	0.20		26
1.4362	2304	< 0.030	23	4	0.3	0.10		25

## Mechanical properties

Table 2 shows the ultimate tensile strength (U.T.S.) and the yield strength (Y.S.<sub>0.2%</sub>) measured on hot rolled plates with thickness in the range 7-20mm. From these results, 450 and 650MPa can be done as minimum values for Y.S.<sub>0.2%</sub> and U.T.S. respectively. The objective to obtain tensile properties twice than the conventional austenitic is reached by combining duplex microstructure with high N level.

Table 2. Room temperature tensile data of 1.4062 hot rolled plates

Thickness	Y.S. <sub>0.2%</sub> (MPa)	U.T.S (MPa)	E (%)
7	548	725	36
12	532	750	36
20	475	689	40

## Corrosion resistance

### Pitting corrosion resistance

#### Cold-drawn wires pitting corrosion resistance in chloride environments

Pitting corrosion is evaluated by an accelerated electrochemical test which determines the pitting potential: the higher the pitting potential, the better the pitting corrosion resistance (potentiodynamic testing with measure of pitting potential for a current density of  $100 \mu\text{A}/\text{cm}^2$ ).

Two types of samples for 1.4062 and 1.4404 grades were tested:

- Industrial rod-wire with a diameter of 5.5mm; the samples are tested after mechanical polishing (paper SiC 1200) and after air ageing for natural passivation (during 24 hours).
- Industrial cold-drawn wire, with 2.3mm and 1mm diameters. The samples are tested with their industrial surface after only a short degreasing.

We used a chlorides containing solution (NaCl 0.86M or 5% weight) at  $35^\circ\text{C}$  and neutral pH; this medium is the solution of the “salt test” (ASTM B117<sup>7</sup>).

The results are given in Figure 1. The lean duplex 1.4062 presents pitting potentials higher than the ones measured for the austenitic 1.4404 for rod and cold drawn wires. In addition, it should be noted that the difference of corrosion resistance between 1.4062 cold-drawn wires of diameters 2.3 and 1mm is due to the roughness difference (1mm diameter wires are smoother and roughness has an influence on pitting corrosion resistance).

#### Rebar pitting corrosion resistance in severe concrete environments

Pitting corrosion potentials have been measured in synthetic, alkaline, carbonated and chlorides containing solutions. The synthetic media were defined to take into account the evolution of the interstitial solution in the vicinity of reinforcement and concrete in time. The solution represents a concrete composition modified over time, with a high content of sodium chlorides. Indeed, the stainless reinforcements are often selected for aggressive environments such as marine conditions.

The results obtained in a containing chlorides carbonated medium at  $\text{pH} = 8$  are given in Figure 2. The values of pitting potential of stainless steels are definitely higher than those measured under the same conditions for traditional steel ( $-350 \text{ mV}/\text{ECS}$ ). Lean duplex stainless steels 1.4362 and 1.4062 which contain low level of Ni and Mo, present pitting potentials higher than the ones measured for the austenitics 1.4301, 1.4404 and 1.4571. In addition, it should be noted that a good correlation is obtained with the PREN (Pitting Resistance Equivalent Number) in these alkaline solutions.

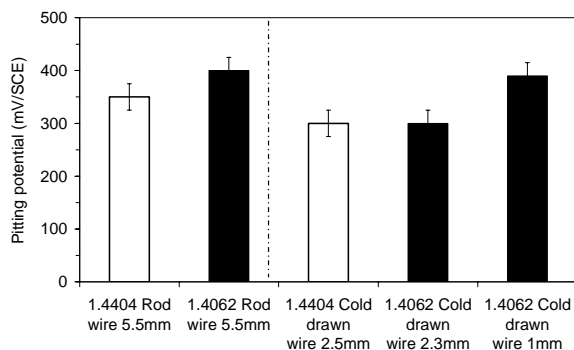


Figure 1. Pitting potential for various grades in neutral medium with an addition of sodium chloride of 50 g/L at  $35^\circ\text{C}$ .

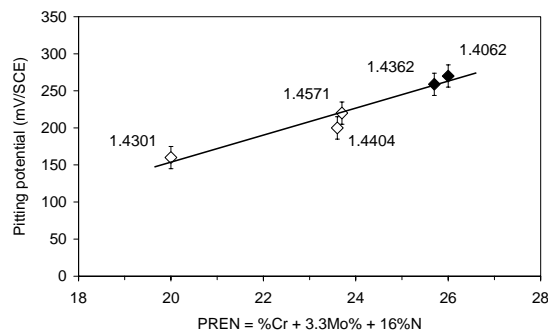


Figure 2. Pitting potential for various grades in the synthetic medium carbonated at  $\text{pH} = 8$  and with an addition of 21 g/L of chlorides.

## Plate pitting corrosion resistance in chloride containing solutions

Pitting corrosion characterizations were performed on polished samples removed from 7mm thick hot rolled plate. Electrochemical tests began 24 hours after sample preparation in order that the passive film may be naturally formed as a result of electrochemical reactions with the atmosphere. After 5000s at the free potential, potentiodynamic curves were plotted at a scan rate of 900mV/hour from -50mV/free potential in the anodic direction until the current density reach 500 $\mu$ A/cm<sup>2</sup>. Pitting potential was measured at a current density of 100 $\mu$ A/cm<sup>2</sup>. After the completion of the electrochemical tests, stainless steel samples were observed by means of an optical microscope

Firstly, pitting potentials were measured in a solution containing 250mg/L of chlorides (NaCl 7.10<sup>-3</sup>M) at pH 5.5  $\pm$  0.1 and 25  $\pm$  0.1°C. The electrolyte was prepared from deionised water (R = 18.2M $\Omega$ ). These experimental conditions are the most aggressive, in respect of pH and chlorides content, encountered for fresh water. Indeed 250mg/L is the maximum concentration of several drinking water standards<sup>8,9,10</sup> and 5.5 is the pH value taken by natural aerated fresh water. With these experimental conditions, 1.4307 and 1.4404 have pitting potential values around 800mV/SCE whereas no pits were observed for both duplex grades 1.4062 and 1.4362 after completion of the electrochemical test (see Figure 3). This indicates that the new duplex grade, with a pitting corrosion resistance higher than the one of 1.4307, will be suitable in environments containing limited chlorides content as drinking water.

Then critical pitting temperature (CPT) was measured according to ASTM G150-99 standard<sup>11</sup>. The specimen is exposed to a 1M NaCl (35.5g/l chlorides) solution and heated from 1  $\pm$  1°C to CPT at a rate of 1°C/min. 60s before the start of the temperature scan, the specimen is anodically polarized at 700mV/SCE. The current is monitored during the temperature scan, and the CPT is defined as the temperature at which the current density exceeds 100 $\mu$ A/cm<sup>2</sup> for 60s. Pitting on the specimen is confirmed by a visual examination performed at the end of the test. The CPT for the new duplex grade 1.4062 is higher than the one of conventional austenitic stainless steels 1.4307 and 1.4404 and near from the one of most alloyed austenitic grade 1.4429 (see Figure 4). In the austenitic family, beneficial effect of Cr, Mo and N on CPT value are highlighted. For duplex, the highest value is measured on 1.4362 sample that would indicate a beneficial effect of Ni too.

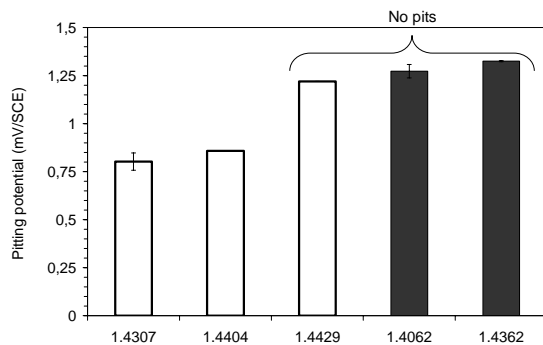


Figure 3. Pitting potential in 250g/L chlorides containing solution at pH 5.5 and 25°C.

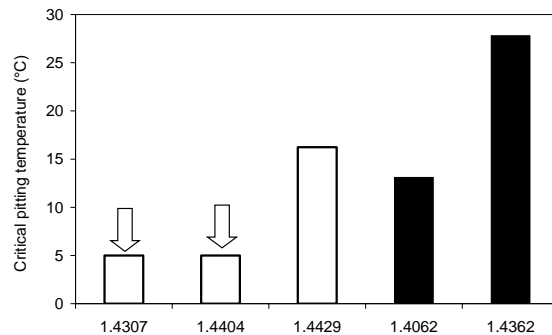


Figure 4. Typical value of CPT according to ASTM G150 standard (vertical arrow indicates that CPT is lower than 5°C)

## Crevice corrosion resistance

Crevice corrosion resistance of 7mm hot rolled plate was investigated by an electrochemical technique. Several potentiodynamic curves were plotted on samples, free of crevice promoting

equipment, with pH values decreased from 3 to 0.5 (controlled by HCl) in order to measure the maximum current density on the active peak. These tests were performed at 20°C in a 2M NaCl (70 g/l chlorides) solution, which corresponds to the expected chloride concentration range inside a crevice. One hour before the beginning of the test and during this test, the solution and the cell are deaerated with N<sub>2</sub>. After 15 minutes at free potential, a fixed potential of -750mV/SCE was applied for 2 minutes in order to reduce the surface species. Then, the potentiodynamic curve was plotted in the anodic direction at a scanning rate of 600mV/hour from -750mV/SCE until the current density reached 500μA/cm<sup>2</sup>. From all the curves plotted for each grade, the maximum current density in the active domain was plotted in function of pH value and depassivation pH (pH<sub>d</sub>) determined at 10μA/cm<sup>2</sup> (see Figure 5). pH<sub>d</sub> corresponds to the onset of an active peak in the potentiodynamic curves.

For the four tested grades, pH<sub>d</sub> values are very similar and equal about 1.6. Considering a mechanism of crevice initiation based on general breakdown of the passivity, that means that the high Cr content of the duplex grades allows obtaining a resistance to initiation similar to the one of a 2%Mo containing austenitic grade. On the other hand, for pH values lower than the depassivation pH, the current density decreases with the increase of the Ni and Mo contents. This confirms the beneficial effect of these alloying elements on the resistance to crevice propagation.

### Uniform corrosion resistance

Coupons taken from hot rolled plates were immersed during several 48h periods in stagnant sulphuric acid. The corrosion rate was evaluated by weight loss measurements. The iso-corrosion curves plotted on Figure 6 for both duplex grades and Mo containing austenitic grade 1.4404 are very similar. This confirms the beneficial effect of high Cr content on the uniform corrosion resistance in diluted sulphuric acid.

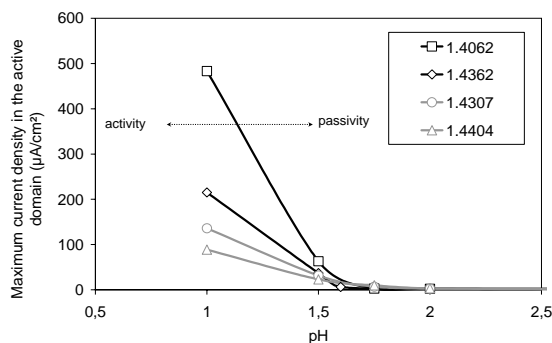


Figure 5. Maximum current density in the active domain versus pH at 20°C in 2 M NaCl.

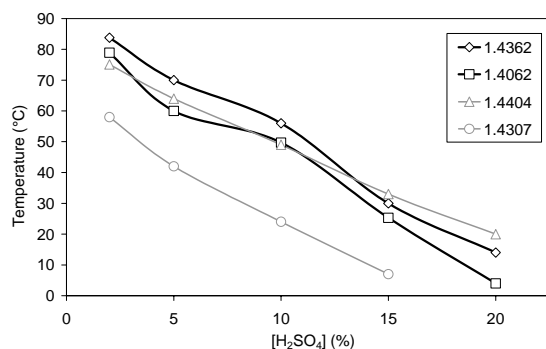


Figure 6. iso-corrosion curves for pure diluted sulphuric acid (corrosion rate = 0.2mm/y).

### Atmospheric corrosion resistance

A5 size coupons removed from 1.4062 hot rolled plates were welded and prepared with different mechanical surface treatments: shot blasted, sand blasted and polished. They were exposed in industrial-urban atmosphere and in rural atmosphere. The aggressiveness of these two locations is classified C2 according to corrosion rates measured on steel, zinc, copper and aluminium reference coupons (see ISO 9226 standard)<sup>12</sup>. Up to now, no signs of localised corrosion have been observed on these specimens after more than one year of exposure.

## Conclusion

By combining low Ni content with N addition and without Mn content increase, a new lean duplex grade EN 1.4062 (UNS S32202) was developed by Industeel and Ugitech.

This low Ni, Mo free grade is less sensitive to fluctuations in raw material prices than the standard austenitic grades.

Cr content higher than 21.5% gives pitting, crevice or uniform corrosion resistance better than 1.4301 or 1.4307 and sometimes similar to 1.4404 or 1.4571.

Due to duplex microstructure and 0.2% N addition, the tensile properties are also very high and about twice the ones of standard austenitic grades.

Finally, 1.4062 is today available on hot rolled plate, bar, rebar and cold drawn wire forms. It presents a very interesting cost/technical performance ratio and appears as a promising alternative to standard austenitic materials, cement, coated or galvanized carbon steels in construction (storage, architecture, bridge ...) or transport applications.

## References

- [1] P. Soullignac and J.-C. Gagnepain: "Why duplex usage will continue to grow", Duplex conference, Grado, Italy, 18 – 20 June 2007.
- [2] J. Peultier, F. Barrau, J.-C. Gagnepain and J. Grocki: "Duplex and superduplex stainless steels for wet FGD », AIRPOL conference, Louisville, Kentucky, USA, June 26-28, 2007.
- [3] S. Jacques and G. Hagi: "Tour Pomerol : eight year experience with duplex 1.4462", Duplex conference, Grado, Italy, June 18-20, 2007.
- [4] S. Jacques, J. Peultier, V. Baudu, B. Chareyre and J.-C. Gagnepain: "Corrosion resistance of duplex stainless steels for thermal desalination plant", IDA conference, Maspalomas, Gran Canaria, Spain, October 21-26, 2007.
- [5] E. Chauveau, M. Mantel, B. Drab, S. Chedal; Stainless Steel World Magazin, July 2006, pp30-33.
- [6] J. Kerr, P. V. T. Sheers and R. Paton: "A new lean duplex stainless steel with a low nickel content", 4<sup>th</sup> european Stainless Steel Science and Market Congress, Paris, 2002.
- [7] "Standard practice for operating salt spray (fog) apparatus", ASTM B117, 2007.
- [8] Guidelines for Drinking Water Quality, World Health Organisation, 1993.
- [9] European Commission Directive on the quality of water intended for human consumption (98/83/EC), 1998.
- [10] United States Environmental Protection Agency (USEPA) requirements based on the National Primary Drinking Water Regulations as amended under the Safe Drinking Water Act of 1996.
- [11] "Standard Test Method for Electrochemical Critical Pitting Temperature Testing of Stainless Steels", ASTM G150-99 standard, www.astm.org, 2004.
- [12] "Corrosion of metals and alloys – Corrosivity of atmospheres – Determination of corrosion rate of standard specimens for the evaluation of corrosivity", ISO 9226 standard, www.iso.org, 1992.

# MECHANICAL PROPERTIES AND CORROSION RESISTANCE OF W BEARING SUPERDUPLEX STAINLESS STEELS

*C. Muñoz, A. Paúl, A. Gallardo, J. A. Odriozola*

*Universidad de Sevilla-CSIC.C, Spain*

## Abstract

Superduplex stainless steels present an excellent combination of mechanical properties and localised corrosion resistance. Their chemical composition is based in high contents of expensive elements such as Ni (~ 7%) and Mo (~4%). Ni and Mo contents can be reduced by alloying with N, V and W while maintaining good corrosion resistance (PRE number above 40) and mechanical properties at room temperature.

The addition of W will not only account for the reduction in the Mo content, it will also lead to enhanced mechanical behaviour, making these alloys good candidates in applications where high strength and high corrosion resistance are required.

In this work we compare the pitting corrosion resistance in chloride media and mechanical properties at room temperature of several experimental alloys with the standard SAF 2507 superduplex stainless steels. The chemical composition of the experimental alloys has the following percents: Cr 25%, Ni 7%, Mo 1-3.8%, N 0.4-0.5% and W 0-6%. The other alloying elements are maintained with the same concentration as in the SAF 2507 stainless steel.

## Introduction

Duplex and superduplex stainless steels have an excellent combination of mechanical properties and corrosion resistance. These properties rely on a microstructure formed by approximately equal parts of austenite and ferrite, its morphology and chemical composition. [1]. The first duplex stainless steel had a nominal chemical composition of 22% Cr, 5% Ni and high N content, up to 0.17%. Second generation of duplex alloys included Mo to a maximum of 3% and 0.2%N to increase the pitting corrosion resistance of 2205 type. 22Cr-5Ni-3Mo stainless steels are typically employed in the food industry and off-shore applications [2]. Third and, until now, last generation of duplex stainless steels, known as superduplex, have higher contents on Cr, Ni Mo and N whose typical composition is of 25Cr-7Ni-4Mo-0.3N. These have the best resistance to pitting corrosion than 2205 grades and good mechanical resistance with high elastic limit that allow for material costs reduction. These alloys are increasingly used in many applications as paper and chemical industry, chemical products transport and petroleum and gas manufacturing as well as in off-shore structures [3,4].

The corrosion resistance of duplex stainless steels is described by the Pitting Resistance Equivalent (PRE), which takes into account the influence of the alloying elements in the pitting potential of the stainless steels. Originally

$$\text{PRE} = \% \text{Cr} + 3.3\% \text{Mo} \quad (1)$$

Later, nitrogen was included in the PRE value; the pitting resistance equivalent accounting for nitrogen is designed as PREN and is given by

$$\text{PREN} = \% \text{Cr} + 3,3\% \text{ Mo} + x\% \text{ N} \quad (2)$$

where x varies between 16 and 30 depending on the steel type, chemical composition and the heat treatment of the duplex stainless steels.

As research on duplex stainless steels proceed, other elements needed to be included in the PREN expression, this is the case of tungsten, W. Some author name the new PRE including W as PREW, the influence of W in the PREW is related to Mo but weights half the value of that [5,6].

$$\text{PREW} = \% \text{Cr} + 3,3(\% \text{ Mo} + \frac{1}{2}\% \text{ W}) + x\% \text{ N} \quad (3)$$

Duplex stainless steels can be regarded as superduplex if its PRE number (PREN or PREW) has a value above 40. Tungsten is usually added above 2% to enhance the pitting resistance increasing the passive potential range and the crevice corrosion resistance in hot chlorine solutions. This is due to the migration of W to the passive layer where it forms  $\text{WO}_3$  which is insoluble in water. In neutral chlorine solutions  $\text{WO}_3$  interacts with other oxides increasing the passive layer stability [7].

The main pitfall of duplex stainless steels is their tendency to form the hard and brittle  $\sigma$  phase. It has been confirmed that W levels between 1 and 3% difficults the formation of intergranular  $\sigma$  phase, but it still can precipitate inside the grains in intragranular form. It is thought that this is due to the diffusion of W and Mo to the grain boundaries. Usually, addition of W is accompanied by an equal reduction in Mo in such a way that W + Mo are bellow 5 to 6% [8].

In this work we have studied new superduplex stainless steels with reductions in Mo content by substitution of this element with increasing contents of W. Standard SAF 2507 (EN 1.4410), 25% Cr, 7% Ni, 4% Mo y 0.3% N, duplex alloy will serve as reference. Mechanical properties and pitting corrosion resistance will be determined by standard methods to compare the new alloys with the standard one.

## Experimental

The chemical composition must be such that the  $\alpha$  and  $\gamma$  volume fractions are about 50/50 and to avoid the precipitation of secondary phases that might negatively affect the alloy properties:  $\sigma$ ,  $\chi$  nitrides and carbides. Also C and S will be maintained as low as possible since they enhance the precipitation of undesirable phases. The design of the alloys has been carried out using the Schoeffler equations [9] which take into account the effect of W and N.

$$\text{Ni}_{\text{eq}} = \% \text{Ni} + 30\% \text{C} + 0,5\% \text{Mn} + 30\% \text{N}$$

$$\text{Cr}_{\text{eq}} = \% \text{Cr} + \% \text{Mo} + 1,5\% \text{Si} + 0,72\% \text{W}$$

Experimental 500 g ingots are fabricated using an induction centrifugal furnace (LECOMELT 6.6  $\mu\text{p}$  VAC) with controlled atmosphere of  $\text{N}_2$  at a pressure of 2 bar.

As-cast alloy ingots are soaked at 1050°C during 1 hour to homogenise the microstructure. Chemical composition was measured by glow discharge optical emission spectrometry

(GD-OES) and elemental analysis for light elements, table 1 gives the chemical composition of the four experimental alloys. Volume fraction of austenite and ferrite were measured using standard metallographic techniques and both phases were determined by X-ray diffraction peaks. Also the PREW number was determined using the equation (3) with a coefficient for N equal to 16, so this will give us the lowest PREW number possible. The values of ferrite % and PREW number are also indicated in table 1.

Table 1. Chemical composition ferrite % and PREW number of experimental superduplex stainless steels fabricated in this work.

	<i>C</i>	<i>Si</i>	<i>Mn</i>	<i>P</i>	<i>S</i>	<i>Cr</i>	<i>Ni</i>	<i>Cu</i>	<i>N</i>	Mo	W	Cr <sub>eq</sub>	Ni <sub>eq</sub>	α %	PREW
<b>SAF 2507</b>	0.015	0.56	0.24	0.02	0.0093	25.0	7.55	0.32	0.39	3.69	0.06	23,45	18,86	33	43.6
<b>SD- 1</b>	0.016	0.64	0.19	0.02	0.0059	24.8	7.01	0.30	0.41	2.9	2.15	28,14	18,82	30	44.8
<b>SD- 2</b>	0.018	0.69	0.24	0.02	0.0060	25.2	6.92	0.60	0.46	2.2	4.06	29,89	20,00	23	47.1
<b>SD- 3</b>	0.022	0.82	0.23	0.018	0.0060	24.7	6.97	0.37	0.41	1.2	6.49	30,48	18,95	28	47.7

A specimen is extracted from all the alloys and cold rolled (figure1) to a thickness of 0.5 mm. Cold rolled sheet were heat treated in the same conditions than the as-cast specimens to relieve the stress in the deformed microstructure.

As can be seen in table 1 the ferrite content is low for all the steels prepared, this is probably due to the high Ni content and the low Mn content in all the alloys. Microstructure of as-homogenised and cold rolled specimens is shown in figure 1; these are representative of all the alloys. As-cast microstructure after homogenisation treatment is formed by island of austenite in ferrite grains with solidification structure. Grains are of irregular shape and show no equiaxiality although no preferred direction can be seen in the microstructures. In the microstructure of cold rolled specimens ferrite grains are deformed in the rolling direction giving a fine duplex microstructure with grains strongly elongated in the rolling direction.

Numerous spherical Si-rich inclusions are seen in all the samples. These are caused by the small weight of the ingots which give a low surface to mass (volume) ratio and large interaction with crucible walls during the casting process. Si content is a little bit higher in alloy SD-3.

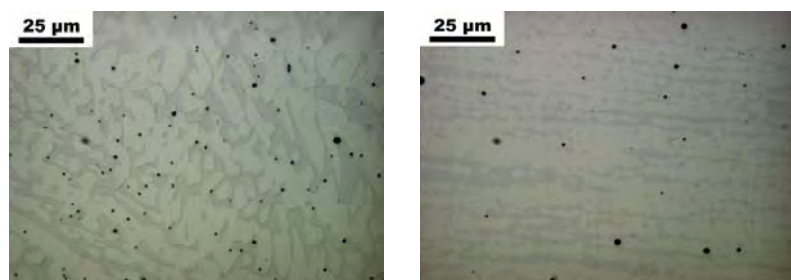


Figure 1. Microstructure of SAF 2507 alloys. Left, as-cast specimen and right, cold rolled alloy. Etching Vilella's

Mechanical properties at room temperature were determined by tension and compression tests. Tension test was performed on the cold rolled specimens while compression tests were done on the as homogenised ones.

Pitting corrosion resistance was determined in as homogenised specimens by cyclic potentiodynamic experiments in 3.5 wt. % NaCl water solution.

## Results and Discussions

X-ray diffraction results, figure 2, show the characteristic peaks of the austenitic and ferritic phases in the alloys. No other crystalline phases were detected.

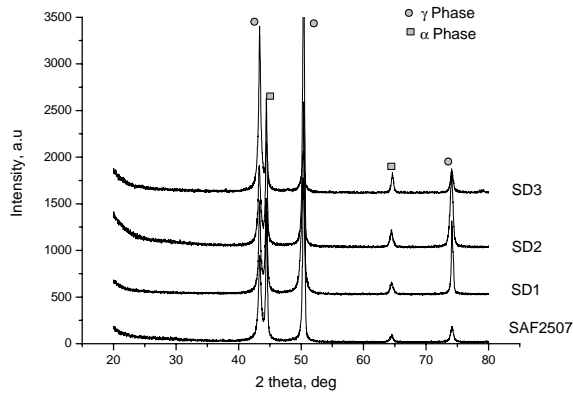


Figure 2. X-ray diffraction for the alloys.

Table 2 show the tension test results. Experimental superduplex alloys have a higher maximum tensile stress than the standard SAF 2507 alloy.  $R_{max}$  value for SD3 is three times that of the 2507 type alloy.

Table 2. Results for tension test to the alloys. \* These alloys fractured outside the calibrated zone

Alloy	$R_{max}$ (MPa)	Elongation (%)
SAF2507	1151	30.08
SD1*	2787	ND
SD2*	2740	ND
SD3	3313	12.20

Figure 3 is a bar diagram of the  $R_{max}$  value for the alloys, it is evident from the graph that alloying with tungsten to 6.49% enhances the mechanical properties. Figure 4 is a comparison of the stress-deformation curves for reference and SD1 alloys. The increase in the mechanical resistance is accompanied by a proportional decrease in the elongation (the data for those specimens could not be calculated because fracture was outside the calibrated area).

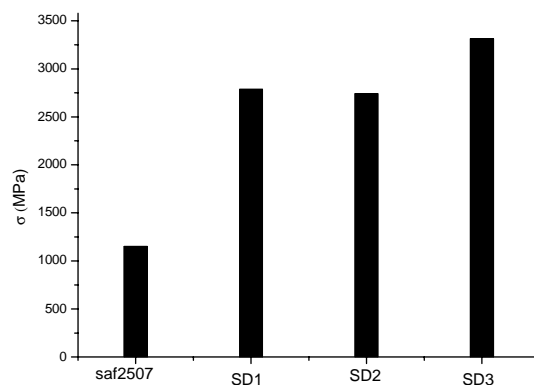


Figure 3. Bar diagram of  $R_{max}$  for the experimental alloys in this work.

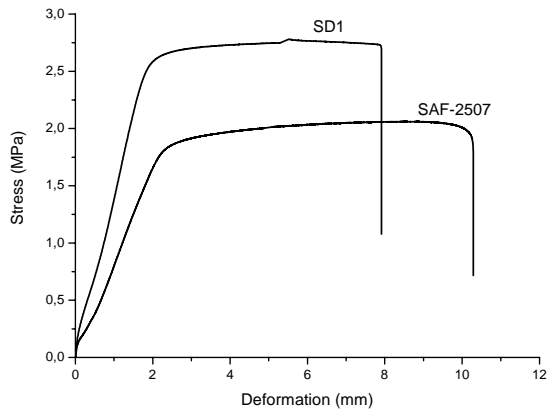


Figure 4. Stress-deformation curves for alloys SAF2507 and SD1 under tension load.

Compression test results are plotted in figure 5. Stress-strain curves indicate that there is a similar behaviour between alloys SAF-2507 and SD1 (their curves are parallel) while a different trend is encountered for SD2 and SD3 alloys. Those differences in trend during the compression tests can be due to the precipitation of W rich phases in the  $\gamma$ - $\alpha$  grain boundary.

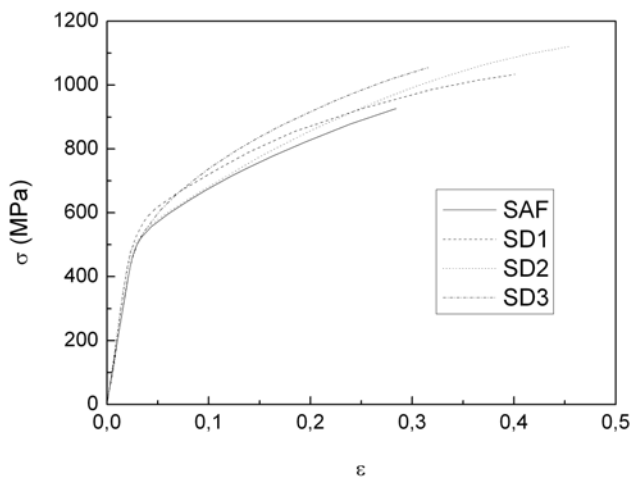


Figure 5. Stress-strain compression curves for the alloys studied in this work

Results indicate that decreasing Mo and increasing the W content enhances the mechanical resistance both in tension and compression tests. Tension tests indicates that there is an increase in the elastic limit data as the W content is increase. Also, the higher the W content the higher the maximum resistance of the specimen. However, the compression test does not indicate that differences in the elastic limits. That behaviour is due to the different microstructure of the specimens. Tension tests were made on cold rolled specimens in the rolling direction so that the microstructure was of elongated grains in the tension direction while the compression experiments were done on the as-cast microstructure that shows no preferential direction. The different microstructures give a different mechanical behaviours.

Regarding the corrosion results, table 3 and figure 6, alloy SAF-2507 has a slightly higher pitting potential than the other samples but the differences are not relevant and all the alloys have similar pitting resistance as it was expected from the PREW numbers.

Table 3. Pitting potential for the superduplex alloys studied in this work.

Muestra	$E_{pic}$ (V)
SAF2507	1,14
SD-1	1,08
SD-2	1,10
SD-3	1,11

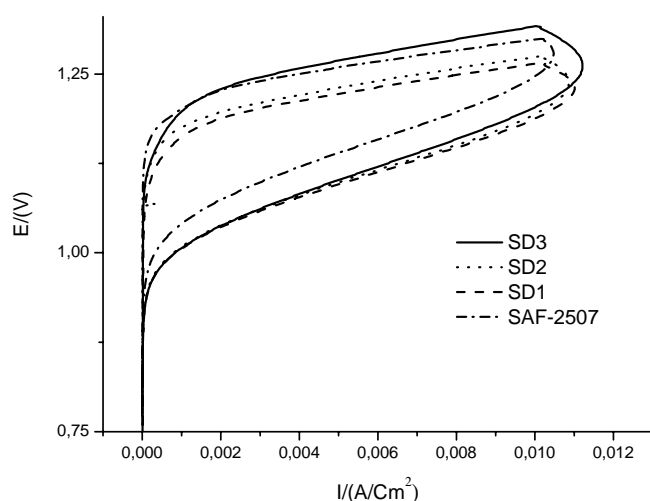


Figure 6. Cyclic potentiodynamic polarization curves for the superduplex alloys studied in this work.

## Conclusions

Result in this work indicate that substitution of Mo by W in superduplex stainless steel will lead to better mechanical resistance while maintaining similar resistance to pitting corrosion.

The mechanical properties are related to the microstructure of the alloys and, thus, to their thermomechanical history. Cold rolled specimens have higher elastic limit as W increases in the alloy.

The pitting potential in chlorine media in all the as-cast alloys is similar and differences between them are negligible.

## References

- [1] S. Jana, 1<sup>st</sup> European Stainless Steel Conference, v.3 p.343-348.
- [2] Dionicio, E. Rev. Inst. investig. Fac. minas metal cienc. geogr, jul. 1999, vol.2, no.3, p.11-21. ISSN 1561-0888.
- [3] R. N. Gunn. Abington, Duplex Stainless Steels. Microstructure, Properties and Applications. Publishing. 1997.
- [4] J. Foct, T. Magnin, P. Perrot, J.-B. Vogt, in: J. Charles, S. Bernhardsson (Eds.), Duplex Stainless Steels '91, Beaune, 1991, p. 49.
- [5] J. E. Truman. Conf. Proc. UK Corrosion. Birmingham **2** (1987) 11.
- [6] L.F. Garfias-Mesias, J.M. Sykes, S.S. TUC Corrosion Science **38** (1996) 1319-1330.
- [7] C. J. Park, H. S. Kwon, Corrosion Sci. 44 (2002) 2817
- [8] B.W.Oh, J.I.Kim et al, 1<sup>st</sup> European Stainless Steel Conference, v.3 p.59-64
- [9] E.A. Schoefer, Welding J. **53** (1974) 10.

# HIGH TEMPERATURE FORMING OF A SUPERDUPLEX STEEL AND ITS SIMULATION BY TORSION TESTING. COMPARISON BETWEEN SUPERDUPLEX STEELS AT SIMILAR TEMPERATURES AND STRAIN RATES RANGES

*M. Carst<sup>1</sup>, I. Rieiro<sup>2</sup>, F. Peñalba<sup>3</sup>, J. Muñoz<sup>2</sup>, J. Castellanos<sup>2</sup>, O. A. Ruano<sup>1</sup>*

*<sup>1</sup>National Center for Metallurgical Research, Spain, <sup>2</sup>University of Castilla-La Mancha, Spain, <sup>3</sup>INASMET Foundation, Spain*

## **Abstract**

The forming behaviour of a super duplex steel is investigated by means of high temperature torsion tests. The composition of the steel is 23.5 Cr, 5.56 Ni, 3.2 Mo, 0.18 N and balance iron and has a PREN value of 37.1. This type of steel has an application in the production of seamless steel pipes that are used for oil extraction and transport. The torsion was performed at temperatures in the range 850 to 1200°C and strain rates in the range of 2 to 26 s<sup>-1</sup> to characterize the mechanical behaviour of the steel. The torsion tests were used, in addition, to simulate the hot forming of pipes under comparable conditions of temperature, strain rate and strain. The parameters of the Garofalo equation were calculated from the experimental torsion data to describe the deformation behaviour of the alloy at various temperatures and strain rates. A non-linear method, involving an algorithm specifically developed for the treatment of this equation, was used. The high temperature forming of the steel was analyzed by means of energy efficiency maps. In addition, a study of the maximum mechanical stability conditions was made. The intersection region for maximum stability defined by the Liapunov criteria together with the maximum efficiency region allowed determination of the best conditions for the forming process. It is concluded that these conditions were 1000°C at the typical industrial forming strain rates of 10 s<sup>-1</sup>. The results for this steel are compared with those for other superduplex steel with a PREN value of 39.73.

## **Introduction**

An increase in popularity has been observed since the introduction of the first generation of duplex and super duplex steels. These kinds of steels are now used, for instance, for tubes, pipe fittings and valves in the oil extraction and transport. Among other reasons, this is due to a better intergranular and pitting corrosion resistance than other stainless steels. The high content of Cr, Ni and Mo ensures this high protection against corrosion.

The accurate study of the forming behaviour and forming stability of these steels is of great importance since the cost of production can be significantly reduced and its safety can be improved for the applications previously described. In this work, the hot forming behaviour of a super duplex steel is investigated by means of high temperature torsion tests. The results obtained are compared with those obtained for another superduplex steel studied in a previous work, which has a coarser initial grain size and variations in the relative content of Ni, Mo and Mn [1]. For this purpose, the Garofalo equation is used as a constitutive relation and its

parameters are employed to obtain the controlling creep mechanism and the most stable forming regions by means of efficiency stability maps. In addition, the ductility of both steels are evaluated and compared in order to determine the influence of the chemical composition.

## Materials and experimental method

The two steels used in this investigation are commercial grade of type S32760. They were received as a semiproduct in the form of bars 300 mm in diameter with the usual quality conditions and had the following composition:

Table 1. Chemical composition of the superduplex steels.

Composition	%C	%Si	%Mn	%P	%Cr	%Ni	%Mo	%Cu	N
Steel 1	0.025	0.46	1.64	0.014	23.45	5.56	3.25	0.17	0.18
Steel 2	0.03	0.44	0.5	---	24.8	7.0	3.7	---	0.17

The major composition differences between the two steel are the content of Mn, Mo and Ni. Steel 1, can be considered as a superduplex steel since its PREN index ( $PREN = \%Cr + 3.3\%Mo + 16\%N$ ) is 37.1. Steel 2 is also a superduplex steel with a PREN index of 39.73. The simulation of the hot forming behavior of this steel was studied in a previous work by means of torsion and tensile tests [1].

Simulation of the forming process for steel 1 was carried out by means of torsion tests. An induction furnace heats the test sample until the test temperature. This variable is continuously measured by means of a two-color pyrometer. A silica tube with argon atmosphere ensures protection against oxidation. The torsion samples have an effective gage length of  $L = 17$  mm and a radius of  $R = 3$  mm. The samples were deformed in a SETARAM high temperature torsion machine at CENIM. Strain rates varied between 2 and  $26 \text{ s}^{-1}$  and the temperature between 850 and  $1200^\circ\text{C}$ . The mean initial grain size of the as-received steels was  $30 \mu\text{m}$  for steel 1 and  $60 \mu\text{m}$  for steel 2.

## Results and Discussion

### Fitting of the Garofalo equation

Figure 1 a) and b) shows the torsion data for steel 1 and 2 respectively.

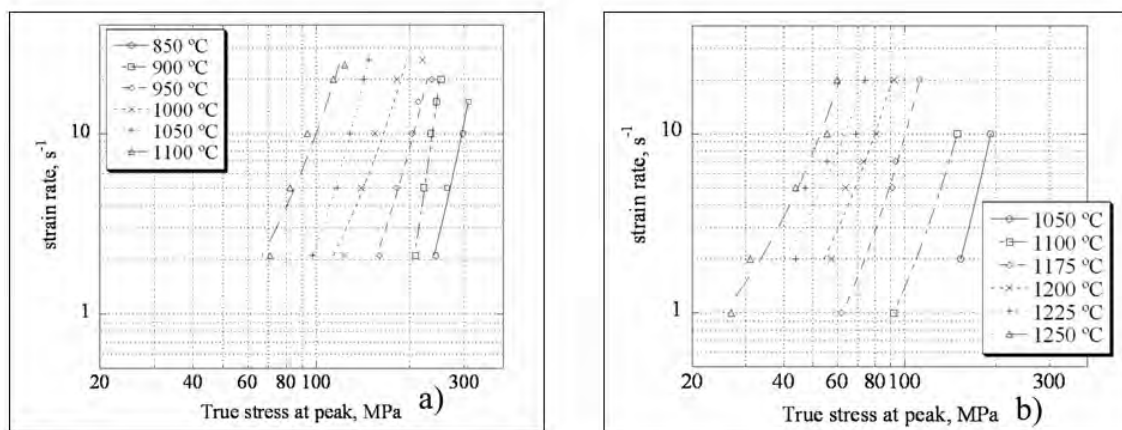


Figure 1. Logarithm of the strain rate vs logarithm of true stress at peak for a) steel 1 and b) steel 2

The Garofalo equation is commonly used to unify the creep data in the entire stress range. It is known that this constitutive relation is capable of heuristically interpreting the creep behavior of polycrystalline materials [2]. This equation is given as follows:

$$\dot{\epsilon} = Ae^{-\frac{Q}{RT}} [\sinh(\alpha\sigma)]^n \quad (1)$$

where  $\dot{\epsilon}$  is the strain rate, T is the absolute temperature,  $\sigma$  is the stress, R is the universal gas constant, Q is the activation energy for deformation, and  $\alpha$ , n and A are material constants. An important characteristic of this equation is that it allows extrapolating the torsion data in order to approach the industrial conditions.

The fitting of the Garofalo equation consists in determining the A, n, Q and  $\alpha$  parameters that best reproduce the torsion data. A non-linear method involving an algorithm specifically developed for the treatment of this equation was used in order to make the parameter identification [3]. The method grants an evaluation of the conditioning of the tests, by means of the *F* function of Snedecor [3].

The Garofalo equation is usually fitted at the maximum of the stress-strain curves (peak value) [4]. For this case, the optimal solutions of the parameters of the Garofalo equation obtained by the algorithm previously described are the following:

$$\text{Steel 1:} \quad \dot{\epsilon} = (5.48 \cdot 10^{11} \text{ s}^{-1}) e^{-\frac{285 \text{ kJ/mol}}{RT}} \left[ \sinh(0.0083 (\text{MPa}^{-1}) \sigma) \right]^{2.99} \quad (2)$$

$$\text{Steel 2:} \quad \dot{\epsilon} = (2.68 \cdot 10^{16} \text{ s}^{-1}) e^{-\frac{447 \text{ kJ/mol}}{RT}} \left[ \sinh(0.0115 (\text{MPa}^{-1}) \sigma) \right]^{3.77} \quad (3)$$

A comparison of equations (2) and (3) reveals that steel 1 shows lower activation energy than steel 2. This can be attributed to the different initial grain size of the steels evolving differently at the various strain rates during testing [5]. This is also the origin of the large values of the activation energy that are usually observed in these steels, much higher than that for iron self-diffusion [6]. Furthermore, the value of n for steel 1 is close to that found in fine grained materials [7]. In contrast the n value for steel 2 is 3.77. This value is close to that associated to a creep mechanics controlled by the climb of dislocations at dislocation pile-ups [8].

### Comparison of hot ductility of the Superduplex Steels

The evolution of the number of turns to failure  $N_f$ , can be considered to be a measurement of the ductility of the material. The evolution of  $N_f$  with temperature and strain rate for steel 1 and 2 are shown in Figure 2 a) and b) respectively.

The low stress exponent of the Garofalo equation for steel 1 suggests that this steel should have better ductility than steel 2 which has a higher stress exponent. This is true at the lower temperatures and strain rates. However, steel 2 shows a jump in ductility at the highest strain rates and temperatures. This surprising behavior needs to be investigated since it could be even associated to an experimental artefact.

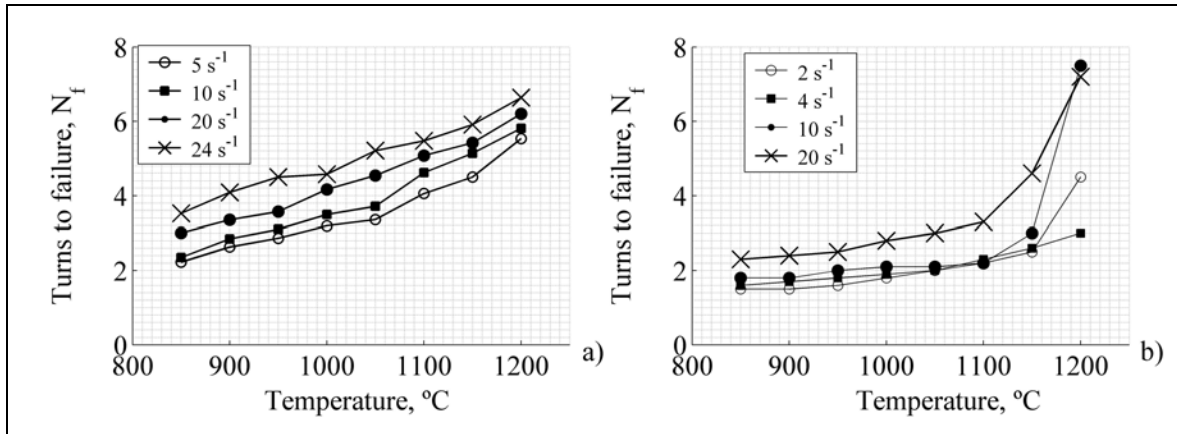


Figure 2. Number of turns to failure with temperature and strain rate for a) steel 1 and b) steel 2.

### Forming stability of the studied steels

The hot forming behaviour of the two steels has been investigated. The hot forming of a metallic material is normally limited by the generation of different processes such as flow localization, cavitations, shear band formation, etc. All these phenomena are a function of the forming variables,  $T$ ,  $\dot{\epsilon}$  and  $\sigma$ . The forming stability maps searches the forming regions where these phenomena are minimized.

According to [9] it is possible to consider the workpiece material under hot working conditions as a dissipater of power. For this situation, the power  $P$ , absorbed by the workpiece during plastic flow can be expressed as:

$$P = \sigma \dot{\epsilon} = G + J = \int_0^{\dot{\epsilon}} \sigma d\dot{\epsilon} + \int_0^{\sigma} \dot{\epsilon} d\sigma \quad (4)$$

Where  $G$  is the dissipater content and represent the power spent in the deformation without changing the internal structure, and  $J$  is the dissipater co-content which is the power spent in the deformation with a change of the internal structure. From this point of view, the Lyapunov stability theorems for the dynamical systems can be applied to the plastic flow in hot deformation [10]:

$$0 < m \leq 1 \quad DMLE = \frac{\partial m}{\partial \ln(\dot{\epsilon})} < 0 \quad (5)$$

$$s \geq 1 \quad DSLE = \frac{\partial s}{\partial \ln(\dot{\epsilon})} < 0 \quad (6)$$

where  $m$  is the strain rate sensitivity and  $s$  is the entropy of the system. These parameters follow the expressions:

$$m = \frac{\partial \ln(\sigma)}{\partial \ln(\dot{\epsilon})} \quad s = \frac{1}{T} \frac{\partial \ln(\sigma)}{\partial (1/T)} \quad (7)$$

Working with these equations and using the Garofalo equation as the constitutive relation, the previous stability criteria can be expressed as [11]:

$$0 < m = \frac{1}{n} \frac{\theta^n}{\sqrt{1 + \theta^n} \sinh^{-1}\left(\frac{1}{\theta^n}\right)} \leq 1 \quad DMLE = \frac{1}{n^2 \Psi} < 0 \quad (8)$$

$$s = \frac{Q}{n^2 RT} \frac{\theta^{\frac{1}{n}}}{\sqrt{1 + \theta^{\frac{2}{n}} \sinh^{-1}\left(\theta^{\frac{1}{n}}\right)}} \geq 1 \quad DSLE = \frac{Q}{n^2 RT} \Psi < 0 \quad (9)$$

$$\Psi = \frac{\theta^{\frac{1}{n}} \sinh^{-1}\left(\theta^{\frac{1}{n}}\right) - \theta^{\frac{2}{n}} \sqrt{1 + \theta^{\frac{2}{n}}}}{\left(\sinh^{-1}\left(\theta^{\frac{1}{n}}\right)\right)^2 \left(1 + \theta^{\frac{2}{n}}\right)^{\frac{3}{2}}} \quad \theta = \frac{\dot{\epsilon}}{A} e^{\frac{Q}{RT}} \quad (10)$$

By means of expression (8) to (10) it is possible to construct stability maps that consist on a two dimensional representation of the previous variables,  $m$ ,  $s$ , DMLE and DSLE with  $T$  and  $\dot{\epsilon}$ . The most stable region is that with the most negative values of the variables DMLE and DSLE.

Figure 3 a) and b) show the contour map for the DMLE functions at strain at peak and for the two superduplex steels.

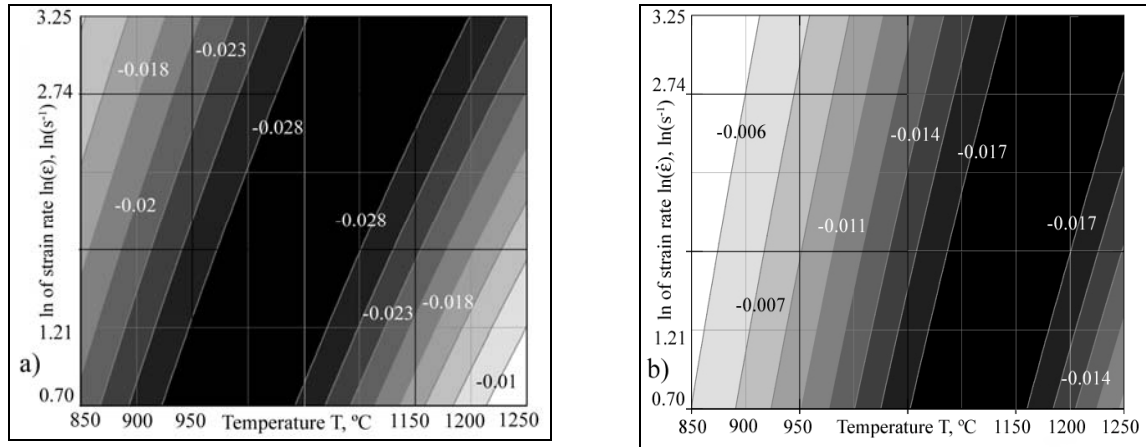


Figure 3. DMLE( $\dot{\epsilon}$ ,  $T$ ) for strain at peak for a) steel 1, and b) steel 2.

Figure 3 a) shows that the maximum stability region for steel 1 is about 1000°C for the typical industrial strain rate of  $10 \text{ s}^{-1}$  (2.3 in the y-axis). For steel 2, figure 3 b) shows that this region is observed at a higher temperature, 1175°C. Therefore, a higher temperature should be applied to steel 2 for a safe industrial forming process.

## Conclusions

- Steel 1 is less creep resistant than steel 2.
- The stress exponent and the activation energy in the Garofalo equation for steel 1 are lower than for steel 2. This may be attributed to the finer grain size of steel 1.
- The ductility of both steels even at the most favorable conditions is relatively low. Steel 1 is clearly more ductile than steel 2 at low strain rates and temperatures.
- At industrial working conditions,  $10 \text{ s}^{-1}$ , the temperature for maximum stability for steel 1 is 175°C lower than for steel 2.

## Acknowledgement

The work was carried out through the Project PBC-05-010-1 from JCCM (Castilla-La Mancha, Spain).

## References

- [1] M. Carsí, J.A. Jiménez, I. Rieiro, O.A. Ruano, “Simulation of the hot forming behavior of a superduplex steel by means of torsion testing”, Proceedings of the III Seminar on Metallurgical Technologies, Barcelona, 2001.
- [2] M.Y. Wu, O.D. Sherby, “Unification of Harper-Dorn and power law creep through consideration of internal stress”, *Acta Metallurgica*, 32, 1984, pp. 1561–1572.
- [3] I. Rieiro, O.A. Ruano, M. Eddahbi, M. Carsí, “Integral method from initial values to obtain the best fit of the Garofalo creep equation”, *J. Mater. Processing Technol.*, 78,1-3, 1998, pp. 177-183.
- [4] J. Adamczyk, M. Carsí, R. Kozik, R. Wusatowski, “Structure forming processes during hot deformation of a C-Mn-V-N steel”, *Steel Research*, 66, 7, 1995, pp. 279-324.
- [5] H.J. McQueen, N.D. Ryan, “Constitutive analysis in hot working”, *Mater. Sci. Eng. A* 322, 2002, pp. 43-63.
- [6] I. Tamura, C. Ouchi, T. Tanaka, H. Sekine “Thermomechanical processing of high strength low alloy steels”, pp. 17-48; 1988, London, Butterworth.
- [7] O.D. Sherby, J. Wadsworth, “Superplasticity: recent advances and future directions”, *Progress in Material Science*, 33, 1989, pp. 169-221.
- [8] J.A. Jiménez, S. Klaus, M. Carsí, O.A. Ruano, G. Frommayer “Microstructure and High Temperature mechanical behavior of the NiAl–27 at.% Cr intermetallic composite”, *Acta Mater.*, 47, 13, 1999, pp. 3655-3662.
- [9] Y.V.R.K. Prasad, H.L. Gegel, S.M. Doraiavelu, J.C. Malas, J.T. Morgan, K.A. Lark, D.R. Barker, “Modeling of dynamic material behavior in hot deformation: Forging of Ti-6242”, *Metall. Mater. Trans. A*, 15, 1984, pp. 1883-1892.
- [10] J.C. Malas, V. Seetharaman, “Using material behavior models to develop process control strategies, *The Journal of the Minerals, Metals and Materials Society*, 44, 1992, pp. 8-13
- [11] M. Carsí, I. Rieiro, J. A. Jiménez, F. Peñalba, O. A. Ruano, “Forming stability of an Al–Ti–Mo intermetallic compound and its dependence on microstructure”, *J. Mater. Processing Technol.*, 143-144, 2003, pp. 416-419.